Supplement to the manuscript "The OH*(3–1) layer emission altitude cannot be determined unambiguously from temperature comparison with lidars" by T. Dunker, submitted to Atmos. Chem. Phys., 2017.

Contents

1 Overview of the data set **2**

2 Effect of fixed altitude and width on temperature comparison **3**

3 OH*(3–1) temperature versus height **5**

4 Appropriateness of a Gaussian weighting function **6**

5 Nightly mean temperature differences and temperature profiles **7**

References **50**

1 Overview of the data set

The .zip–file contains the comma–separated file `lidar_measurements.csv`, which lists all lidar measurements, their duration, and the time when the measurements were started and stopped. Figure S1(a) is a histogram of the commonn measurements per month by GRIPS 9 and the Na lidar at ALOMAR, and Fig. S1(b) is a histogram of the common measurement duration of these instruments.

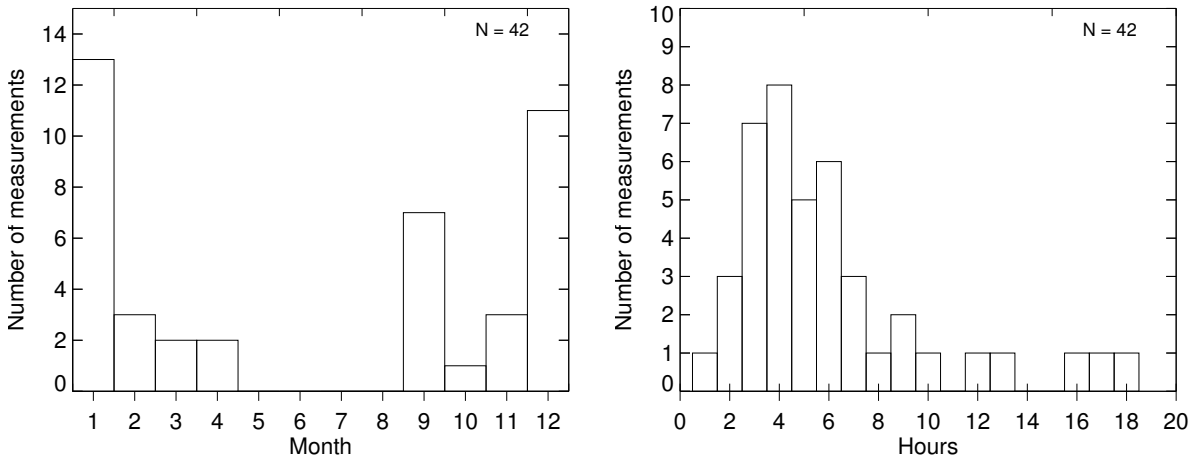

(a) Histogram of common measurements per month.

(b) Histogram of common measurement duration.

Figure S1: Overview of the data set. Fourty–two nights between October 2010 and April 2014 were analyzed. Each night's time series was restricted to periods where both instruments were measuring.

2 Effect of fixed altitude and width on temperature comparison

From Fig. 1 in the main article, it becomes clear that we could obtain well–correlated temperature measurements for a variety of static parameters. It is evident that temperature differences can be quite large (cf. Pautet et al. (2014, Fig. 4) with Fig. S2). These might largely be due to the assumed shape of the OH* layer, and do not necessarily reflect real differences between the instruments. Figure S2 shows that the lidar temperatures appear to be warmer than those measured by GRIPS 9 if we choose a centre altitude of 87.4 km and the optimal full width at half maximum of 9.2 km for each day. Similar pictures emerge if we keep only one parameter fixed (not shown).

The correlation coefficient is quite high, but one has to look at the temperature difference for each day in detail. Then it becomes clear that the correlation coefficient may be misleading for such an analysis. A high correlation coefficient alone neither means good temperature agreement, nor absence of systematic differences, nor valid assumptions underlying the analysis.

Similar to Fig. 2 in the manuscript, Fig. S3 shows the temperature difference for each day, assuming a centre altitude of 87.4 km and a full width at half maximum of 9.2 km. The maximum and minimum temperature differences are 13 K and −19 K. The temperature difference does not have a Gaussian distribution, therefore the mean and standard deviation underestimate the real spread of the data. A better estimate is half the difference between maximum and minimum temperature difference. This means that, under the assumption of a centre altitude of 87.4 km and a full width at half maximum of 9.2 km, the temperature is accurate within ±16 K.

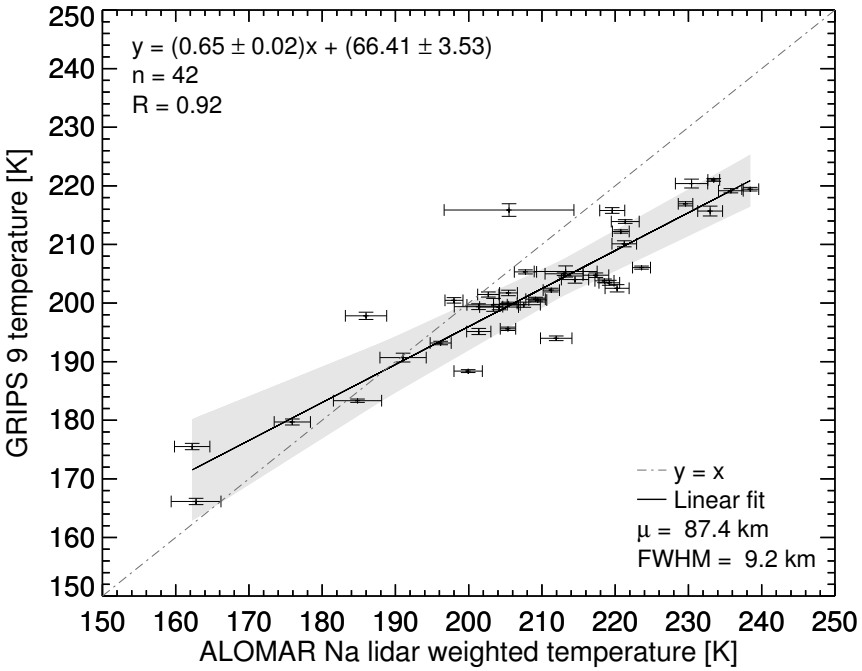

Figure S2: Each day's absolute temperatures for a centre altitude of 87.4 km and a full width at half maximum of 9.2 km, which compares with recent results of Pautet et al. (2014). The grey–shaded area is the 5σ uncertainty of the fit.

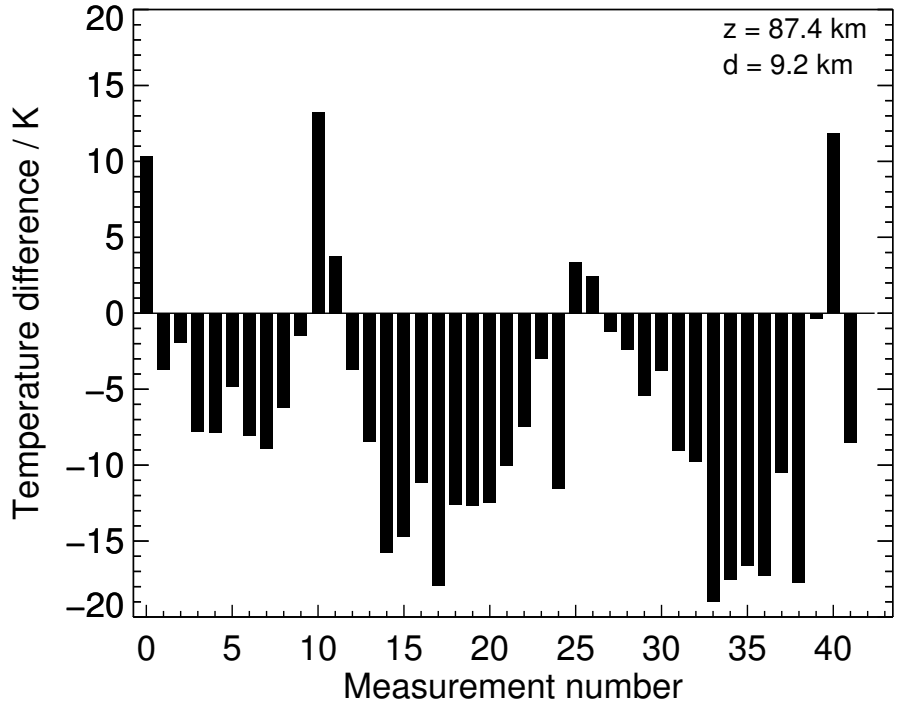

Figure S3: Temperature difference for each day, assuming a fixed a centre altitude of 87.4 km and a full width at half maximum of 9.2 km for each day.

3 OH*(3–1) temperature versus height

Despite different chemistry schemes, the OH* and Na layers should respond similarly to atmospheric dynamics, thus exhibit similar altitude variations: if the centroid height of the sodium layer, which is measured by the lidar, descends or ascends, then the hydroxyl layer will likely behave in a similar way. The analytical model of Swenson and Gardner (1998) supports this view. They further pointed out that temperature variations measured by OH* spectrometers might in part be due to adiabatic motion, despite only small temperature gradients in the mesopause region (Swenson and Gardner, 1998). We found a negative relationship between the OH*(3–1) temperature and the Na layer centroid height (Fig. S4). The lower the Na layer centroid height, the warmer the temperature, which can be expected due to adiabatic warming (Swenson and Gardner, 1998). In this case, the average gradient is $-5.6\,\mathrm{K\,km^{-1}}$.

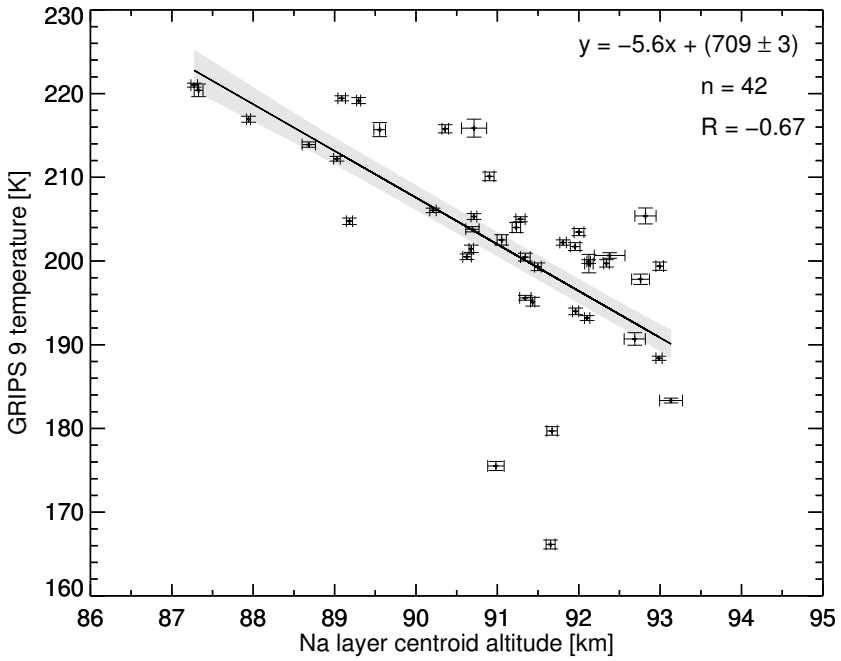

Figure S4: OH*(3–1) rotational temperature measured by GRIPS 9 versus the Na layer centroid height observed by the ALOMAR Na lidar. We performed a linear least-squares fit to the data. The grey–shaded area is the 5σ uncertainty of the fit. Error bars denote the standard errors of the nightly mean.

4 Appropriateness of a Gaussian weighting function

To the best of my knowledge, there is no evidence for OH profiles from satellites which deviate considerably from a Gaussian profile for long averaging times ($\geq$ 1 hour). Furthermore, I am aware of only very few published single satellite–based OH* emission profiles which can be described as double–peaked Gaussians (Winick et al. (2009, Fig. 1), Zhang et al. (2001, Fig. 5)). These profiles are from single overpasses. The other two profiles in Winick et al. (2009, Fig. 1) can be described as Gaussian. Baker et al. (2007, Fig. 6), French and Mulligan (2010), and Noll et al. (2016) all show measured data with essentially Gaussian profile shapes, be it from single overpasses or from averaged data. Thus, to compute an OH*(3–1)–equivalent temperature, the assumption of a Gaussian profile shape can be justified, because the fields–of–view of satellite–based instruments and the GRIPS instrument used here are comparable in size.

Whether the bottom side of the OH* layer, and thus the assumed profile shape, is somewhat steeper than the layer's top side, is probably not of much concern: the weighting factors at these altitudes are very low compared to the peak altitudes, and therefore the resulting temperature will differ little. This has been shown by French and Mulligan (2010). Importantly, such a slight asymmetry would not remove the ambiguity shown in this manuscript. Applying a different weighting function similar to French and Mulligan (2010) would only lead to a different temperature of one of the instruments, thus to different altitudes of the minimum temperature difference. The ambiguity would remain. This study shows that it is the shape of the temperature profile of the mesosphere/lower thermosphere which invalidates the approach of trying to estimate a layer emission height from a temperature comparison with instruments that measure temperature profiles.

5 Nightly mean temperature differences and temperature profiles

Figures S5 to S46 show the several measured quantities for each measurement. Note that the scale of the x–axes varies. Panels (a) show the temperature difference between the nightly mean temperature from GRIPS 9 and Gaussian–weighted temperatures from the Na lidar at ALOMAR as a function of centre altitude and full width at half maximum. Panels (b) of these figures show the nightly mean temperature profile, measured by the Na lidar at ALOMAR, which was used for this manuscript The figures' legends indicate whether the data is from beam 0 or beam 1. The error ranges are of statistical nature (standard error), and are thus not the measurement uncertainties, but a measure of geophysical variability. Panels (c) show the mean temperature profiles from beam 0, beam 1, and the average of these two beams. Panels (d) show the temperature difference between mean profiles of beam 0 and beam 1, which are shown in the respective panel (c). This temperature difference profile is computed as $\overline{T}(z)_{\text{beam 0}} - \overline{T}(z)_{\text{beam 1}}$. On 2 September 2011, 3 September 2011, and 2 September 2013 (Figs. S15, S16, and S30), only one beam was in use, and there is no average or difference to compute.

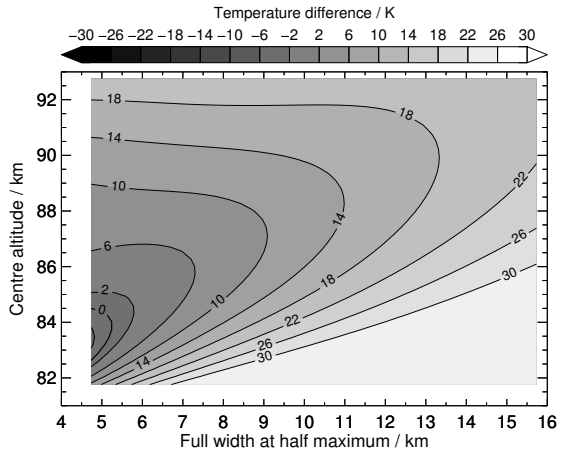

(a) Mean temperature difference between data measured by GRIPS 9 and the Na lidar at ALOMAR.

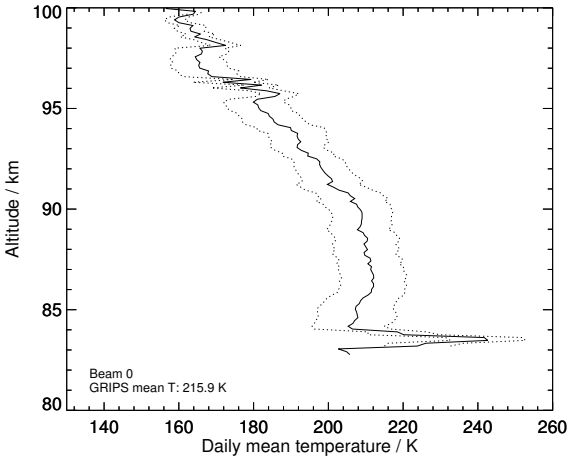

(b) Mean temperature profile from the beam with the best statistics which was used to compute panel (a).

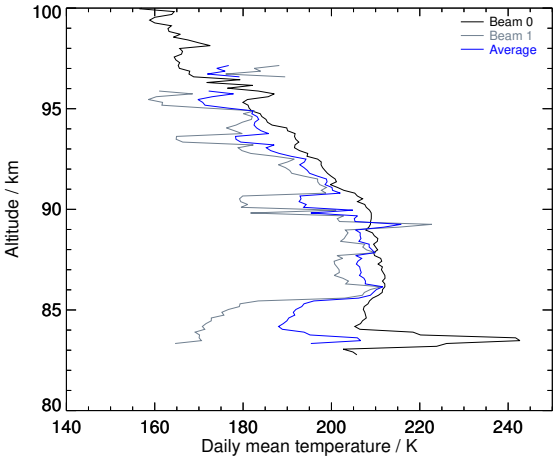

(c) Mean temperature profiles measured by the Na lidar's beam 0, beam 1, and the average of these.

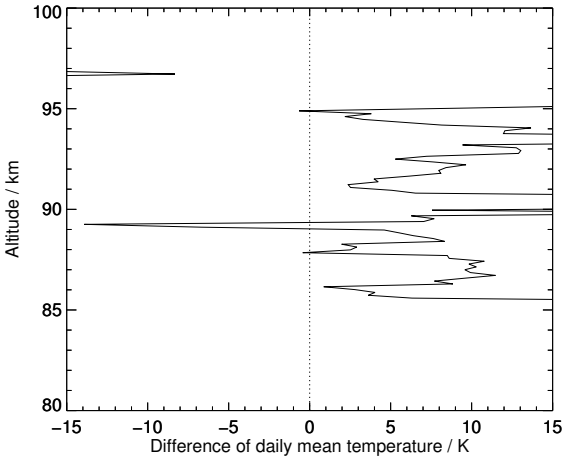

(d) Mean profile of the temperature difference between beam 0 and beam 1, shown in panel (c).

Figure S5: 2010–11–23

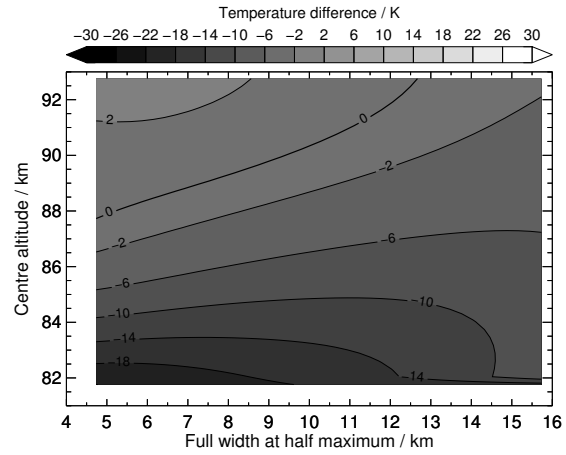

(a) Mean temperature difference between data measured by GRIPS 9 and the Na lidar at ALOMAR.

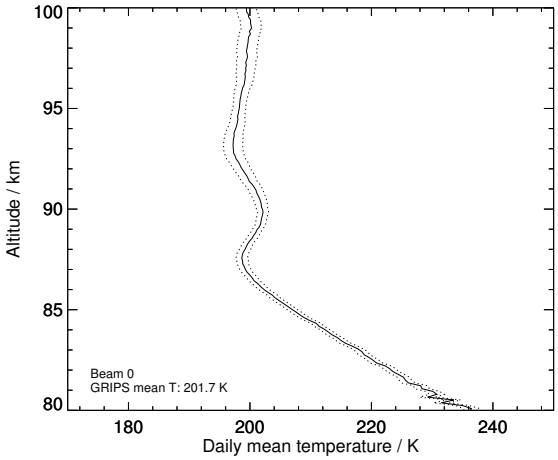

(b) Mean temperature profile from the beam with the best statistics which was used to compute panel (a).

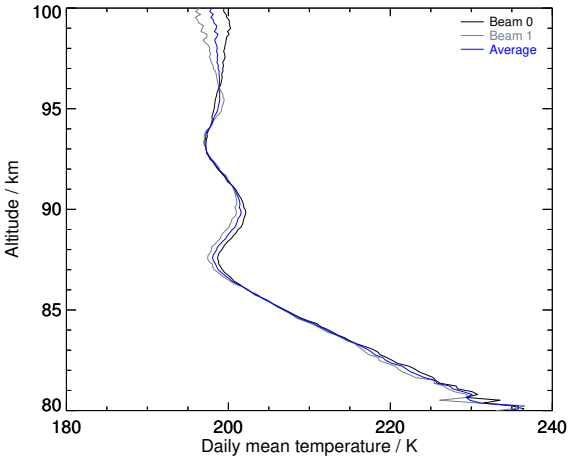

(c) Mean temperature profiles measured by the Na lidar's beam 0, beam 1, and the average of these.

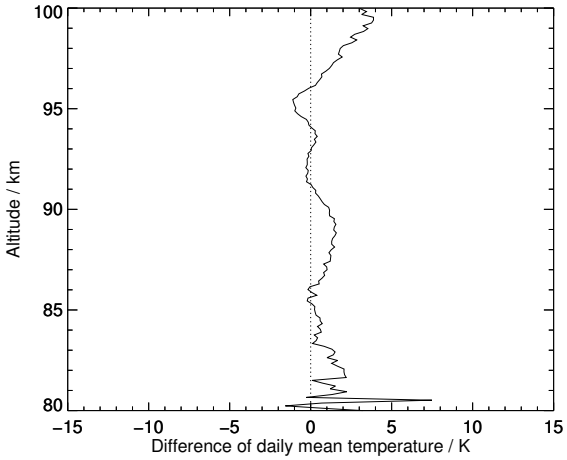

(d) Mean profile of the temperature difference between beam 0 and beam 1, shown in panel (c).

Figure S6: 2010–11–26

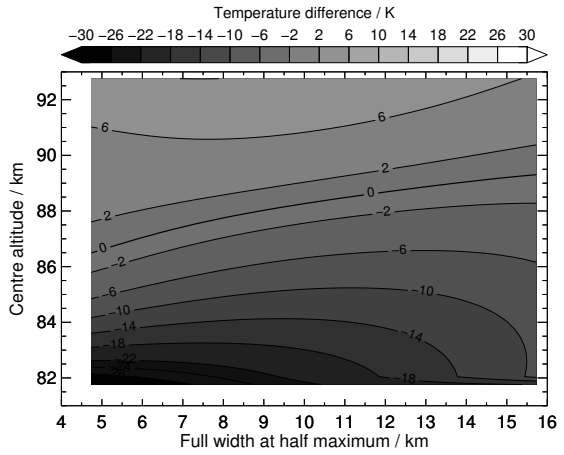

(a) Mean temperature difference between data measured by GRIPS 9 and the Na lidar at ALOMAR.

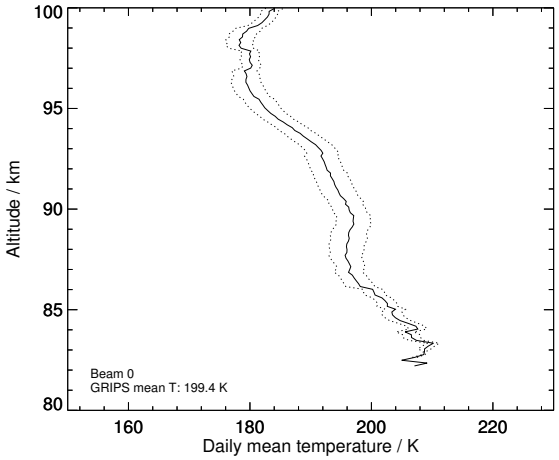

(b) Mean temperature profile from the beam with the best statistics which was used to compute panel (a).

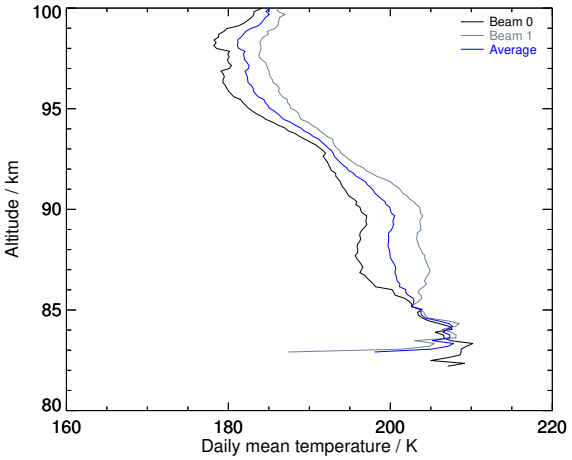

(c) Mean temperature profiles measured by the Na lidar's beam 0, beam 1, and the average of these.

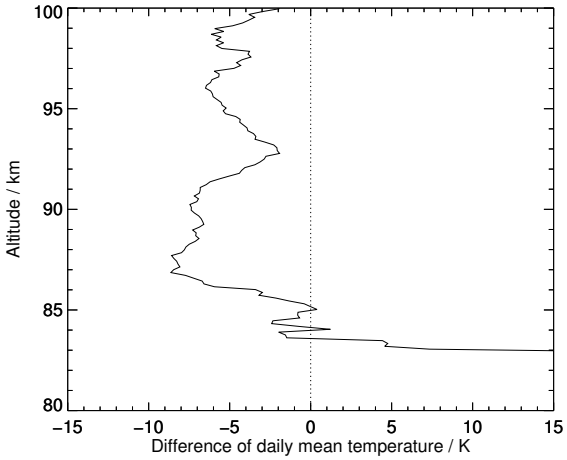

(d) Mean profile of the temperature difference between beam 0 and beam 1, shown in panel (c).

Figure S7: 2010–12–04

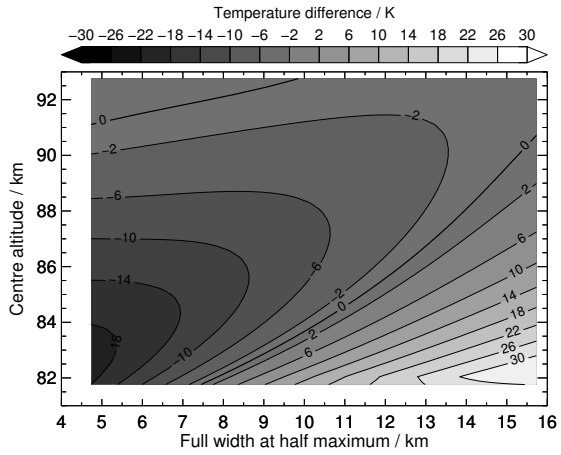

(a) Mean temperature difference between data measured by GRIPS 9 and the Na lidar at ALOMAR.

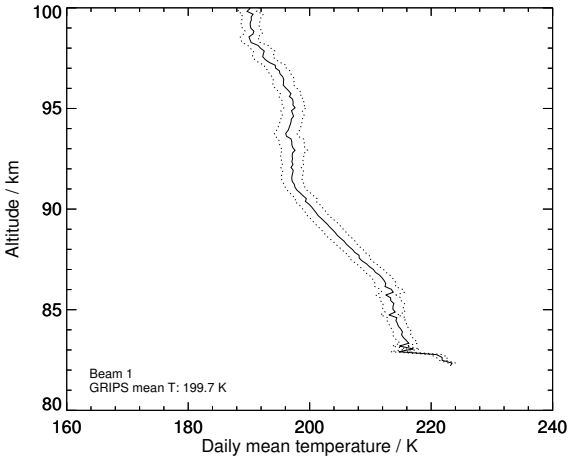

(b) Mean temperature profile from the beam with the best statistics which was used to compute panel (a).

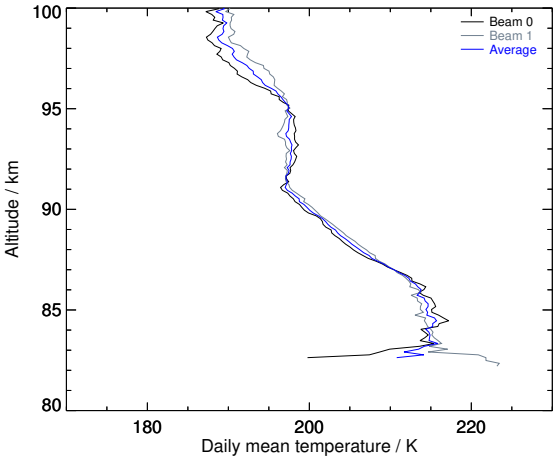

(c) Mean temperature profiles measured by the Na lidar's beam 0, beam 1, and the average of these.

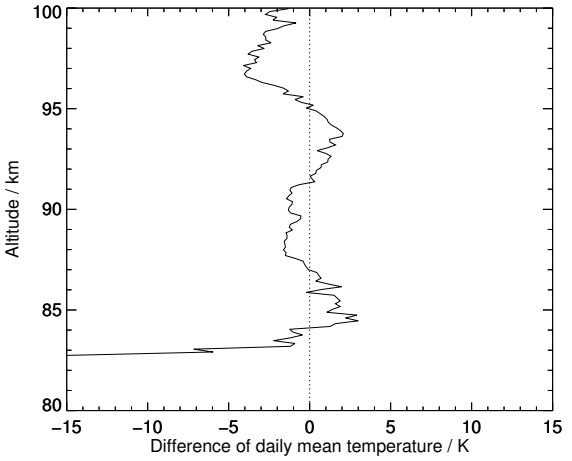

(d) Mean profile of the temperature difference between beam 0 and beam 1, shown in panel (c).

Figure S8: 2010–12–05a

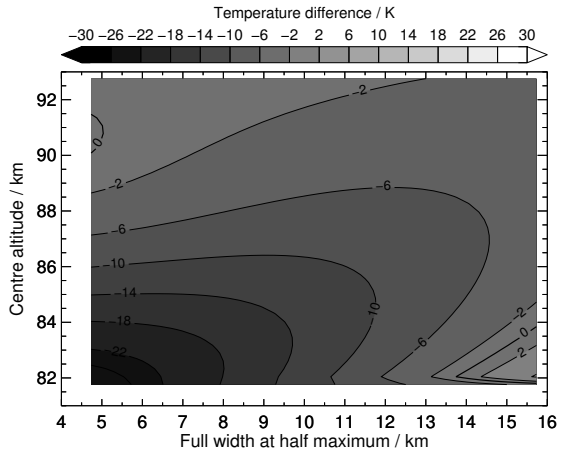

(a) Mean temperature difference between data measured by GRIPS 9 and the Na lidar at ALOMAR.

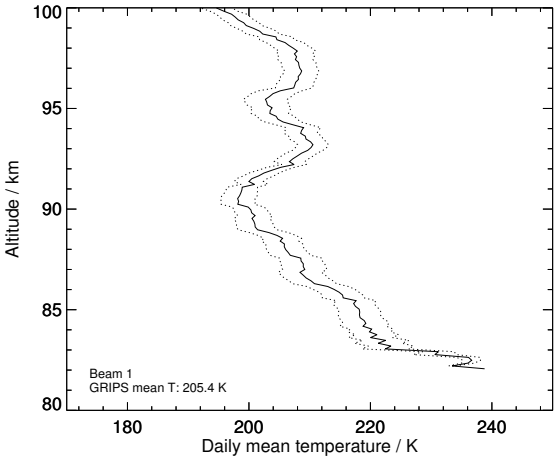

(b) Mean temperature profile from the beam with the best statistics which was used to compute panel (a).

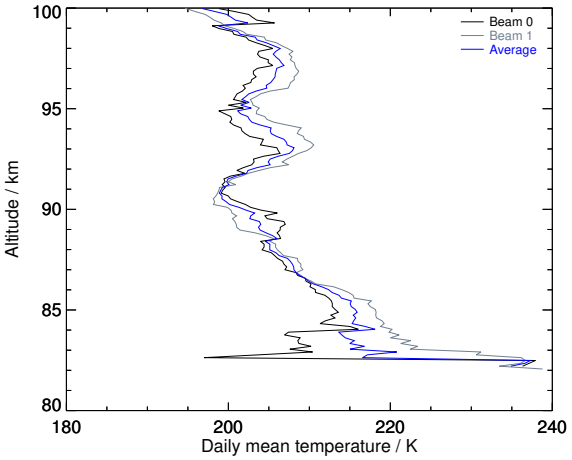

(c) Mean temperature profiles measured by the Na lidar's beam 0, beam 1, and the average of these.

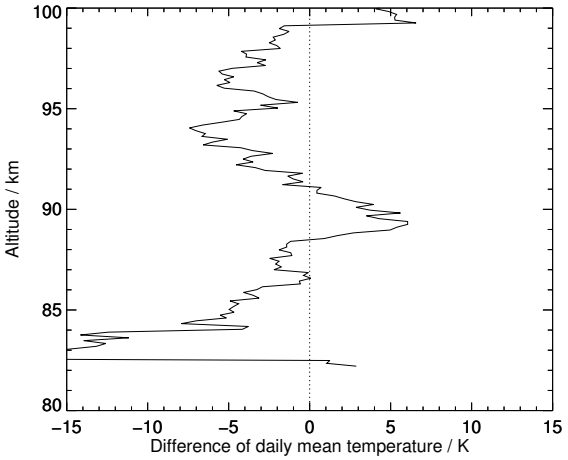

(d) Mean profile of the temperature difference between beam 0 and beam 1, shown in panel (c).

Figure S9: 2010–12–05b

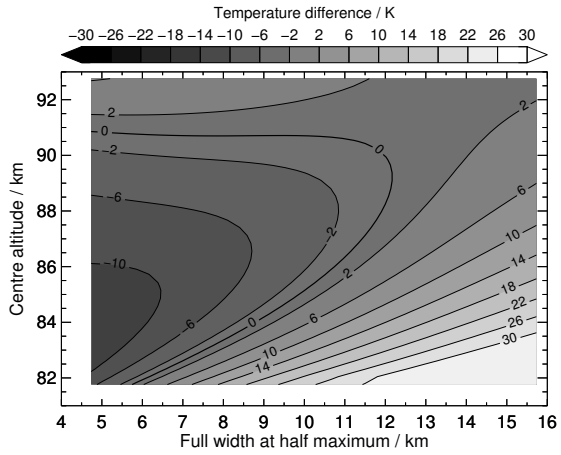

(a) Mean temperature difference between data measured by GRIPS 9 and the Na lidar at ALOMAR.

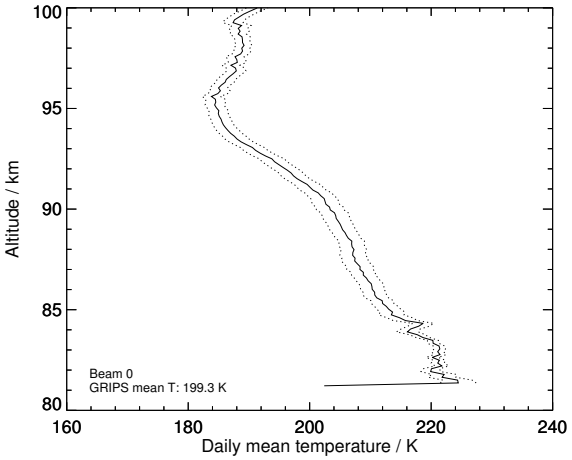

(b) Mean temperature profile from the beam with the best statistics which was used to compute panel (a).

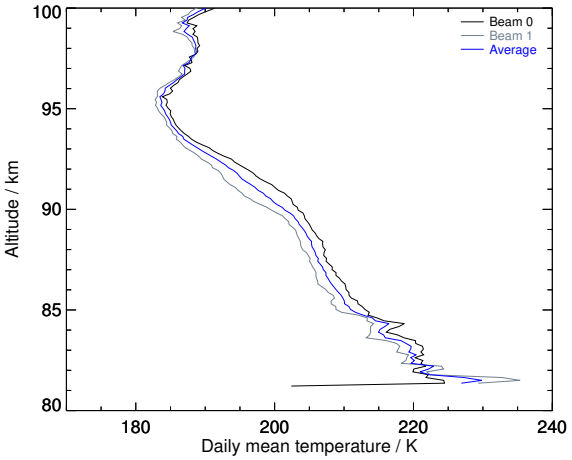

(c) Mean temperature profiles measured by the Na lidar's beam 0, beam 1, and the average of these.

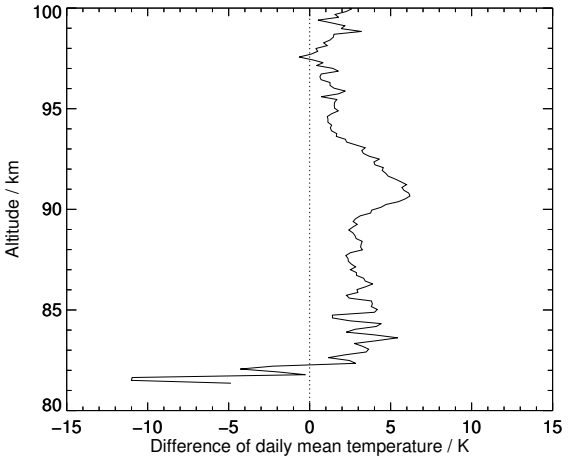

(d) Mean profile of the temperature difference between beam 0 and beam 1, shown in panel (c).

Figure S10: 2010–12–07

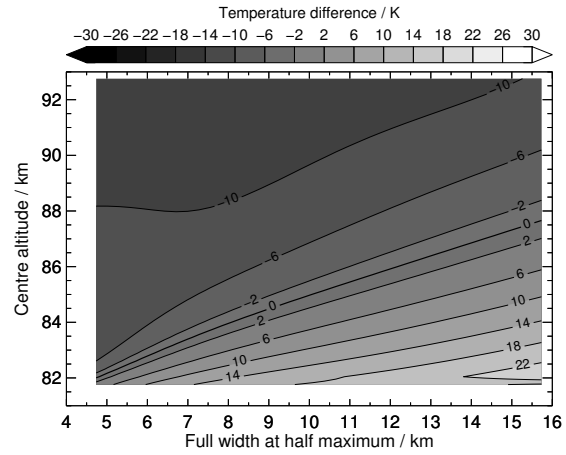

(a) Mean temperature difference between data measured by GRIPS 9 and the Na lidar at ALOMAR.

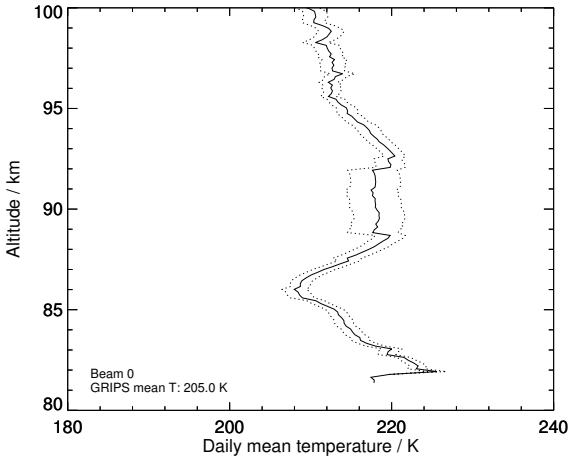

(b) Mean temperature profile from the beam with the best statistics which was used to compute panel (a).

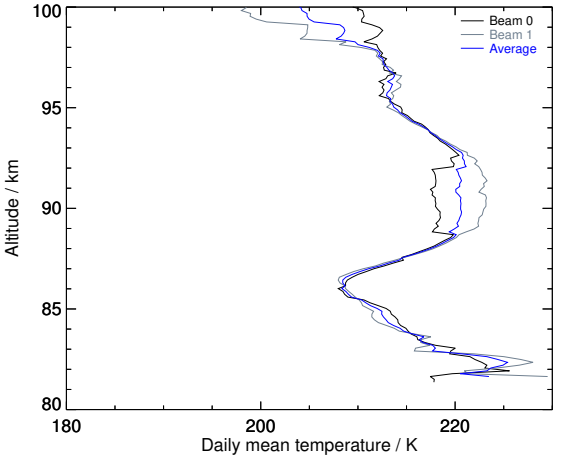

(c) Mean temperature profiles measured by the Na lidar's beam 0, beam 1, and the average of these.

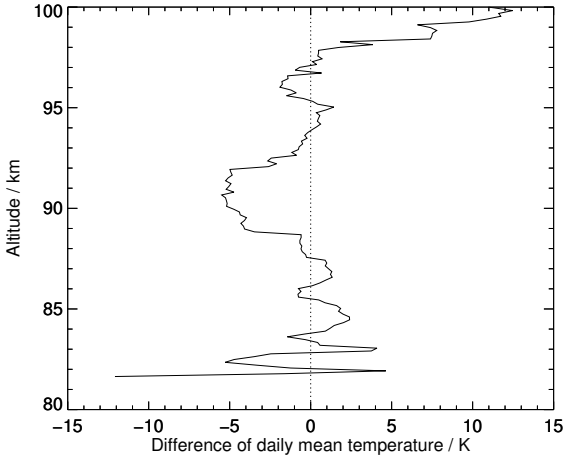

(d) Mean profile of the temperature difference between beam 0 and beam 1, shown in panel (c).

Figure S11: 2010–12–13

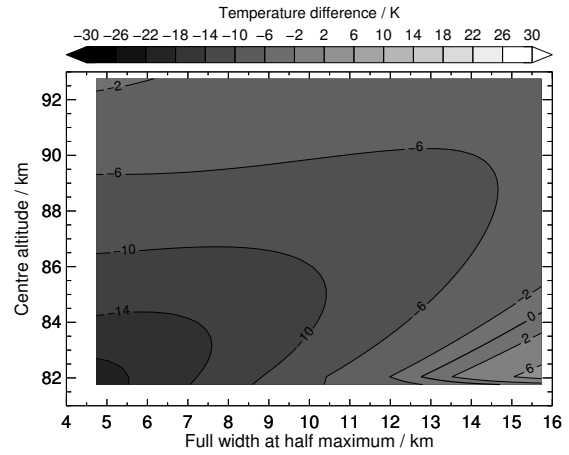

(a) Mean temperature difference between data measured by GRIPS 9 and the Na lidar at ALOMAR.

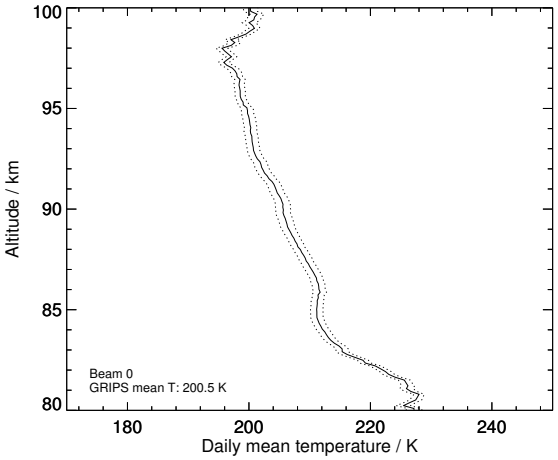

(b) Mean temperature profile from the beam with the best statistics which was used to compute panel (a).

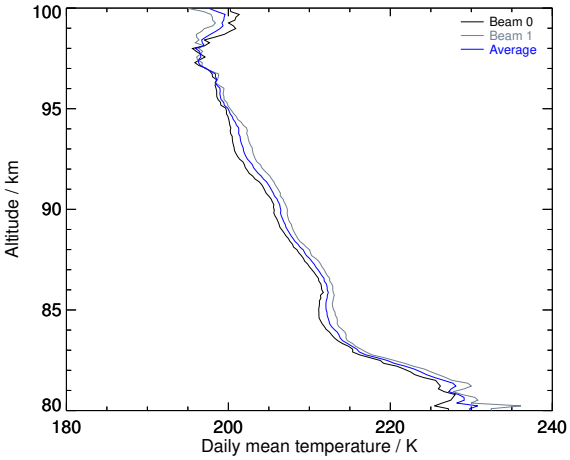

(c) Mean temperature profiles measured by the Na lidar's beam 0, beam 1, and the average of these.

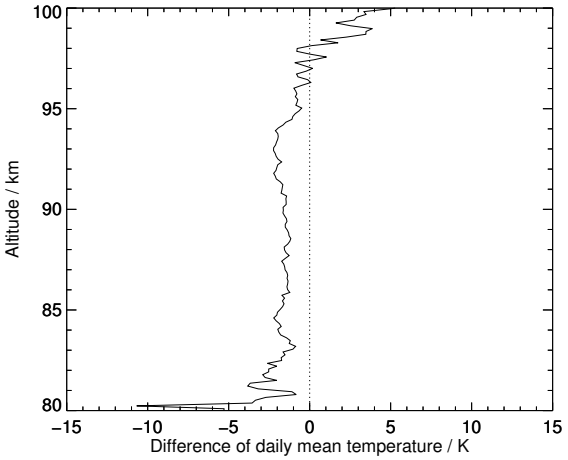

(d) Mean profile of the temperature difference between beam 0 and beam 1, shown in panel (c).

Figure S12: 2011–02–14

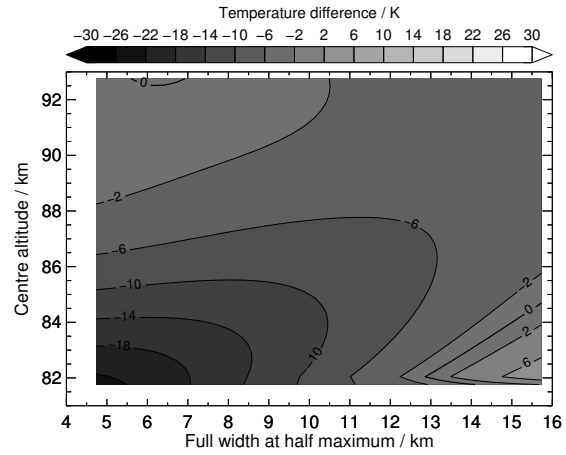

(a) Mean temperature difference between data measured by GRIPS 9 and the Na lidar at ALOMAR.

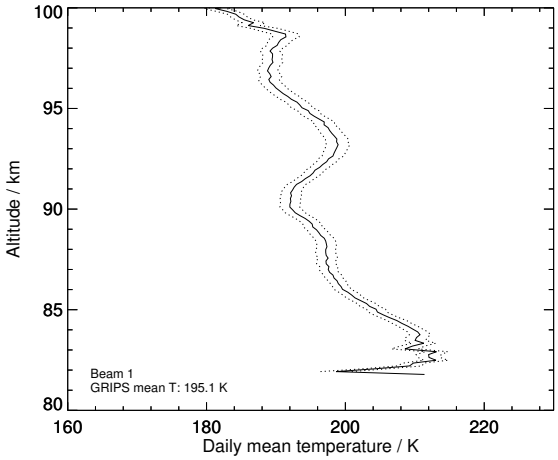

(b) Mean temperature profile from the beam with the best statistics which was used to compute panel (a).

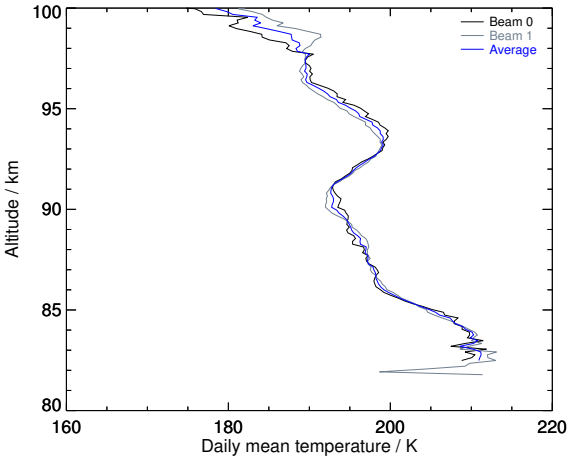

(c) Mean temperature profiles measured by the Na lidar's beam 0, beam 1, and the average of these.

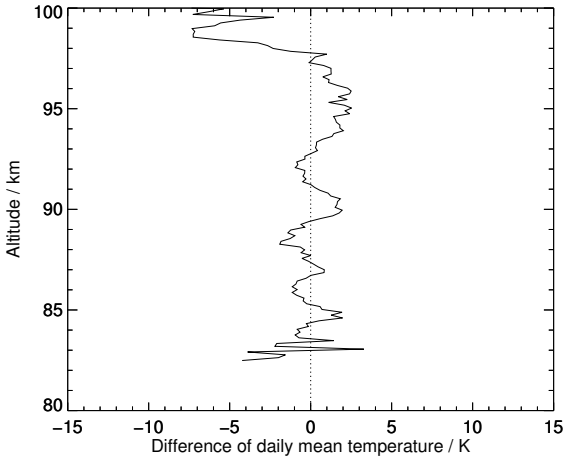

(d) Mean profile of the temperature difference between beam 0 and beam 1, shown in panel (c).

Figure S13: 2011–03–11

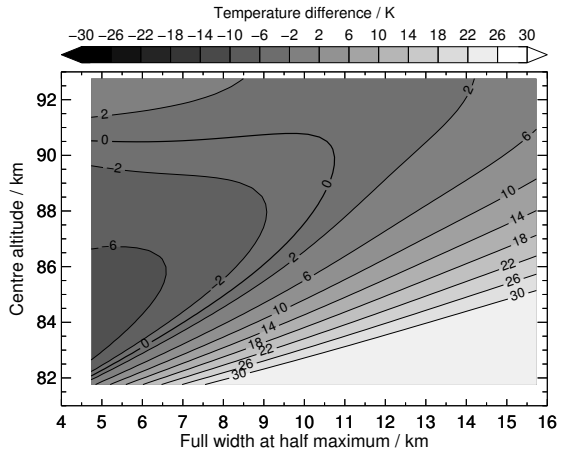

(a) Mean temperature difference between data measured by GRIPS 9 and the Na lidar at ALOMAR.

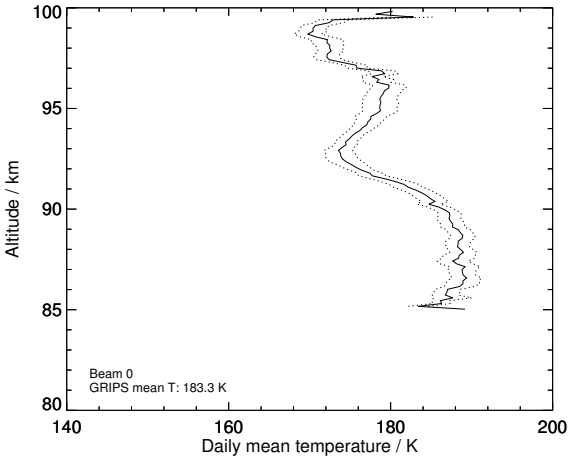

(b) Mean temperature profile from the beam with the best statistics which was used to compute panel (a).

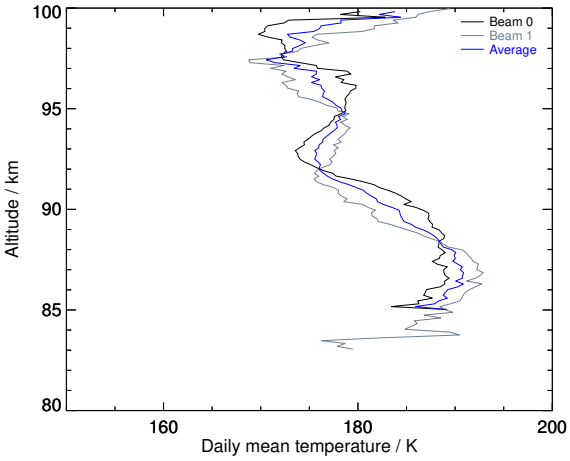

(c) Mean temperature profiles measured by the Na lidar's beam 0, beam 1, and the average of these.

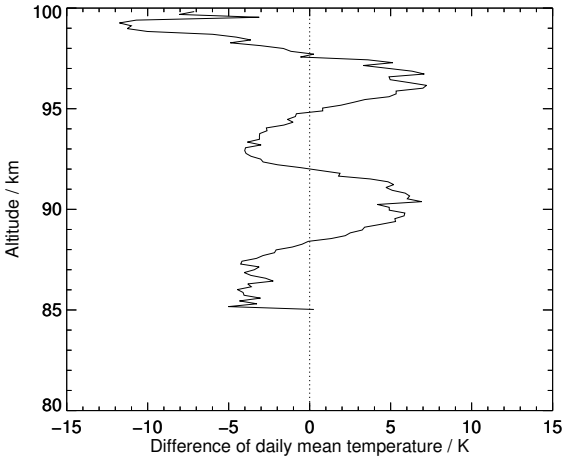

(d) Mean profile of the temperature difference between beam 0 and beam 1, shown in panel (c).

Figure S14: 2011–04–05

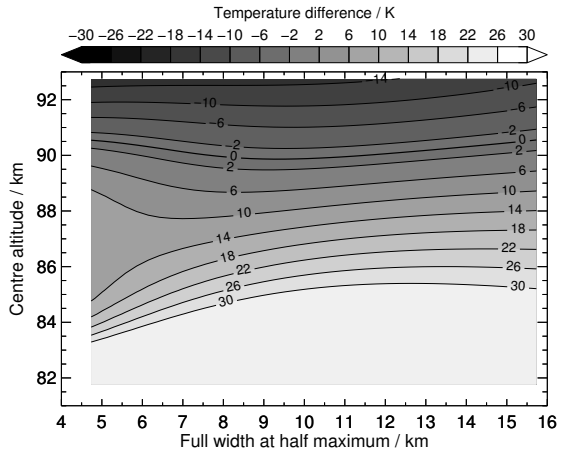

(a) Mean temperature difference between data measured by GRIPS 9 and the Na lidar at ALOMAR.

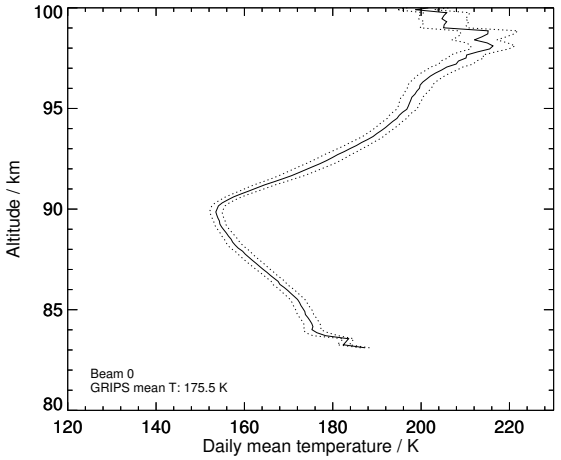

(b) Mean temperature profile from the beam with the best statistics which was used to compute panel (a).

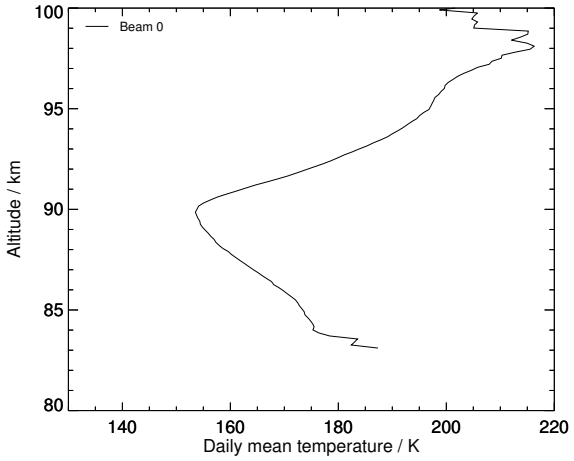

(c) Mean temperature profiles measured by the Na lidar's beam 0, beam 1, and the average of these.

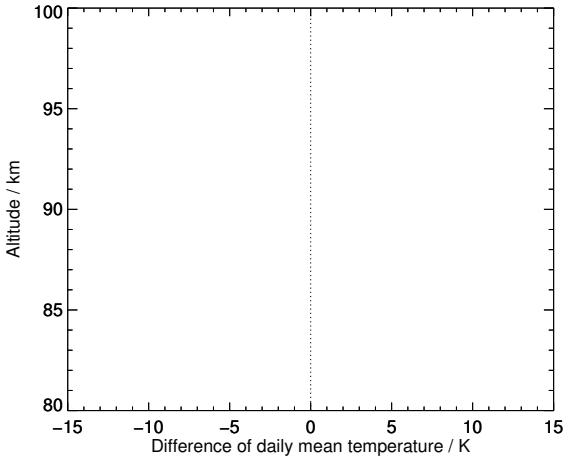

(d) Mean profile of the temperature difference between beam 0 and beam 1, shown in panel (c).

Figure S15: 2011–09–02

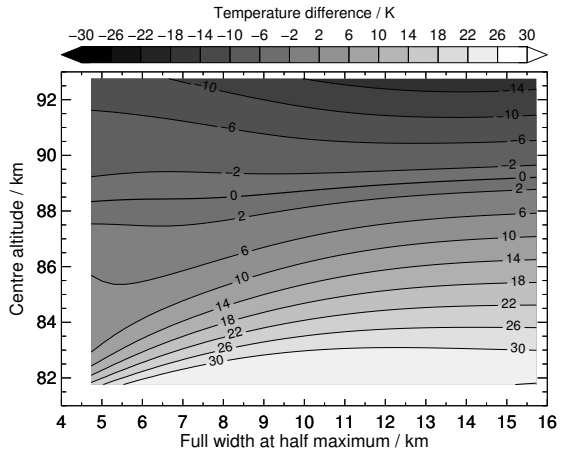

(a) Mean temperature difference between data measured by GRIPS 9 and the Na lidar at ALOMAR.

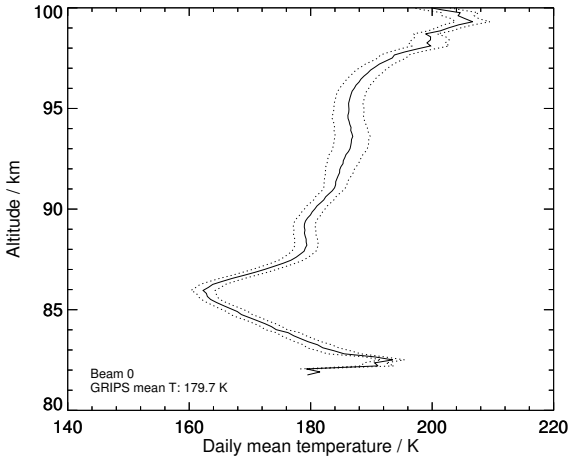

(b) Mean temperature profile from the beam with the best statistics which was used to compute panel (a).

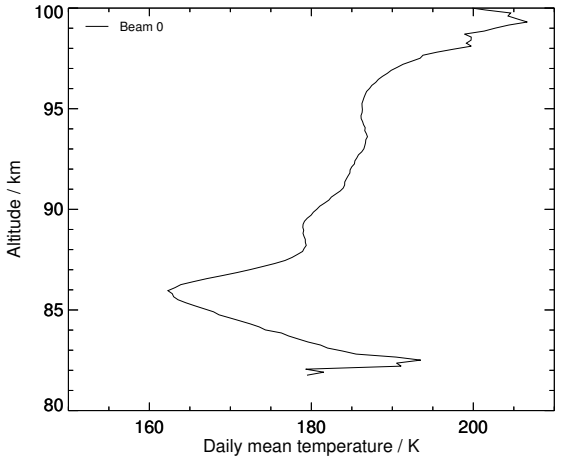

(c) Mean temperature profiles measured by the Na lidar's beam 0, beam 1, and the average of these.

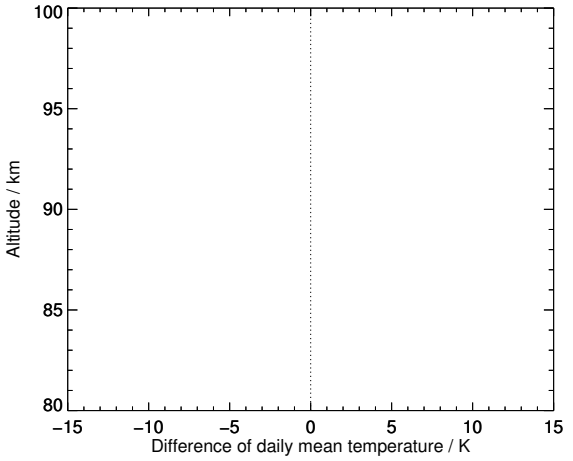

(d) Mean profile of the temperature difference between beam 0 and beam 1, shown in panel (c).

Figure S16: 2011–09–03

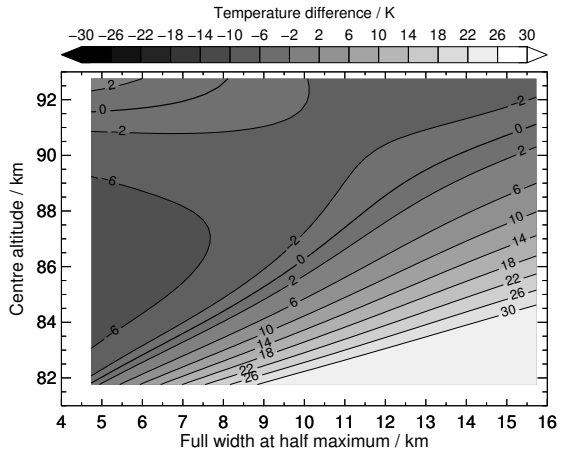

(a) Mean temperature difference between data measured by GRIPS 9 and the Na lidar at ALOMAR.

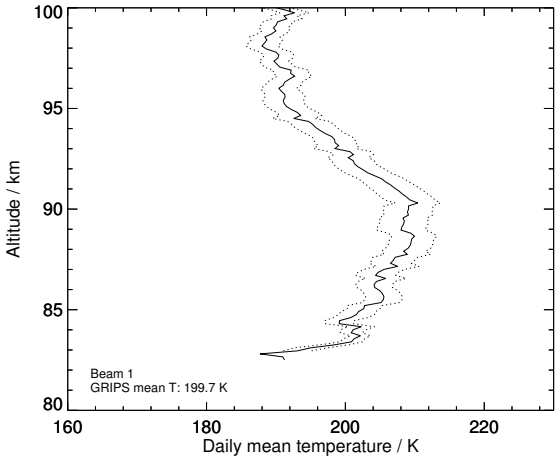

(b) Mean temperature profile from the beam with the best statistics which was used to compute panel (a).

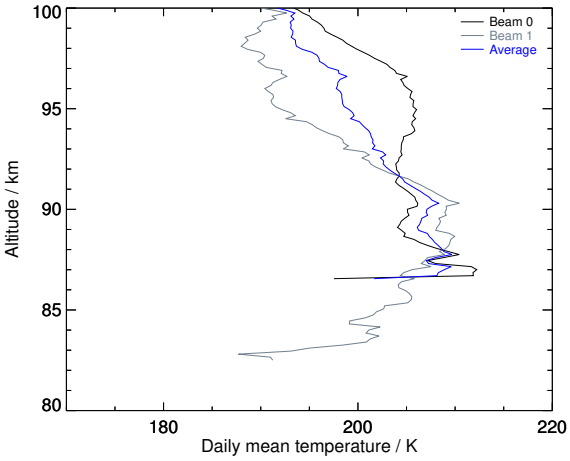

(c) Mean temperature profiles measured by the Na lidar's beam 0, beam 1, and the average of these.

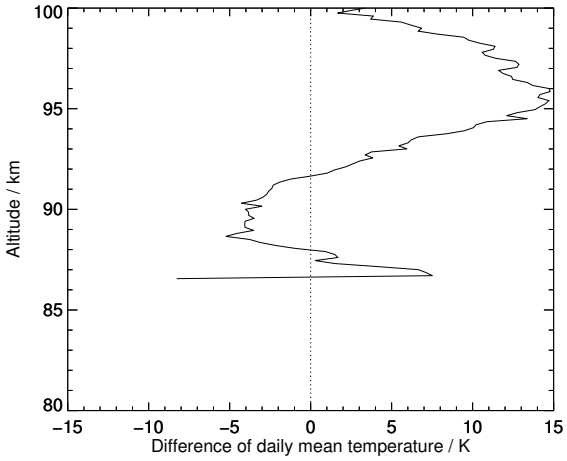

(d) Mean profile of the temperature difference between beam 0 and beam 1, shown in panel (c).

Figure S17: 2011–10–11

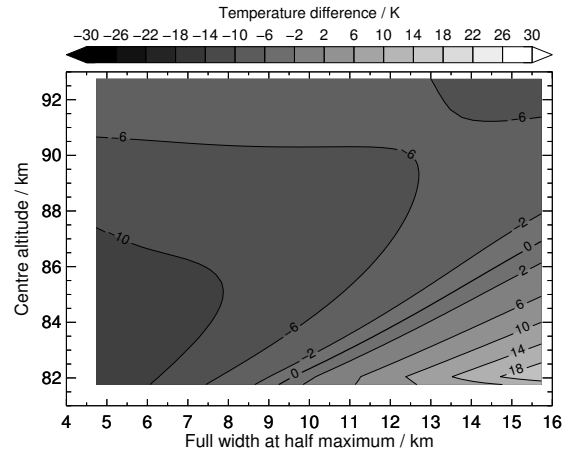

(a) Mean temperature difference between data measured by GRIPS 9 and the Na lidar at ALOMAR.

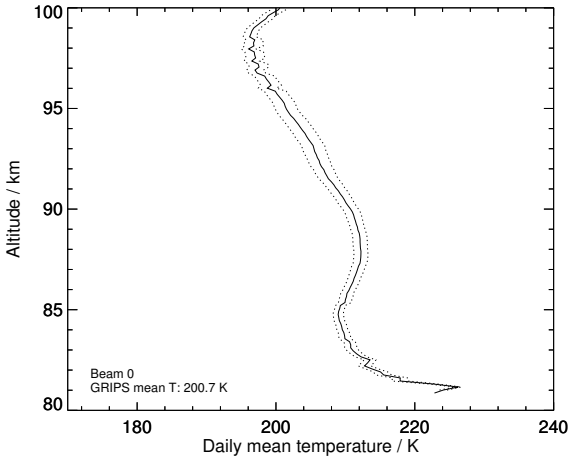

(b) Mean temperature profile from the beam with the best statistics which was used to compute panel (a).

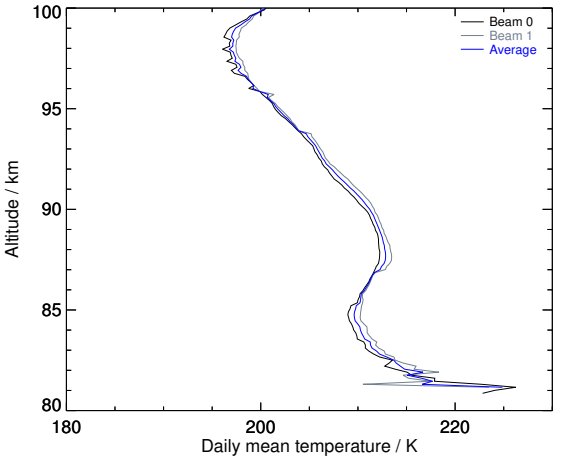

(c) Mean temperature profiles measured by the Na lidar's beam 0, beam 1, and the average of these.

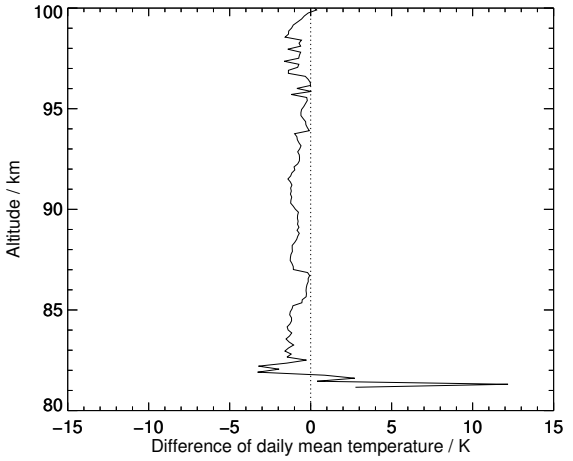

(d) Mean profile of the temperature difference between beam 0 and beam 1, shown in panel (c).

Figure S18: 2011–12–08

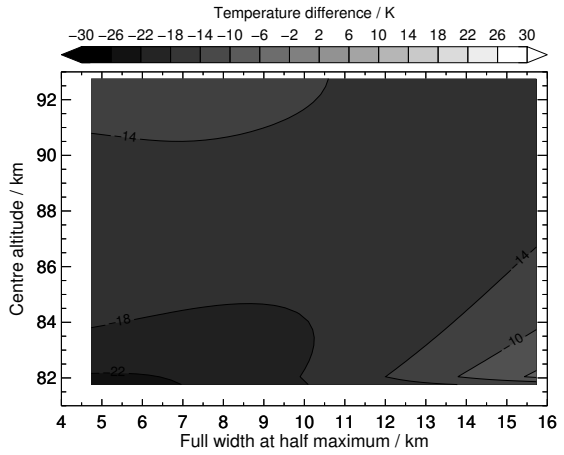

(a) Mean temperature difference between data measured by GRIPS 9 and the Na lidar at ALOMAR.

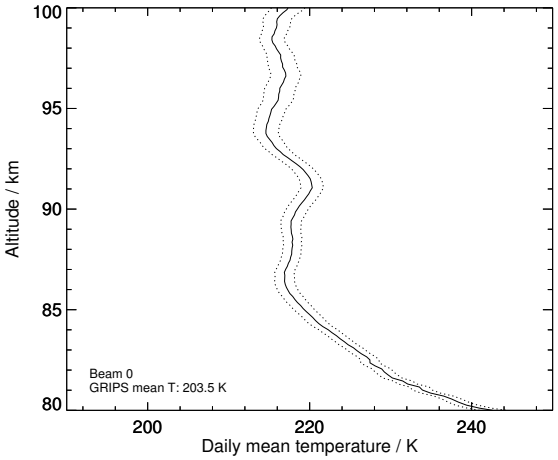

(b) Mean temperature profile from the beam with the best statistics which was used to compute panel (a).

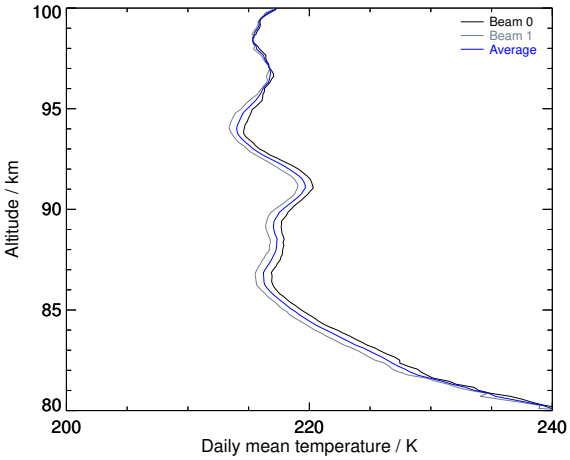

(c) Mean temperature profiles measured by the Na lidar's beam 0, beam 1, and the average of these.

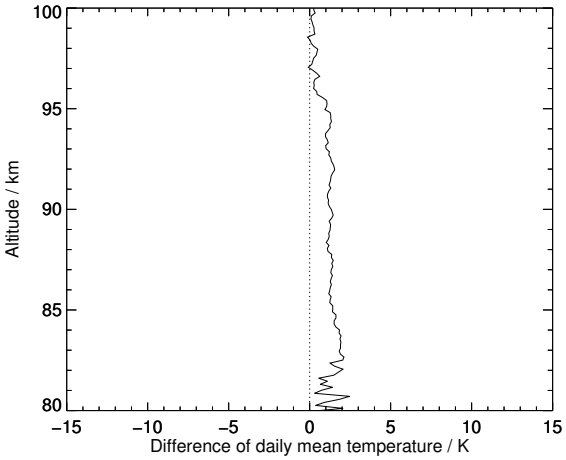

(d) Mean profile of the temperature difference between beam 0 and beam 1, shown in panel (c).

Figure S19: 2011–12–09

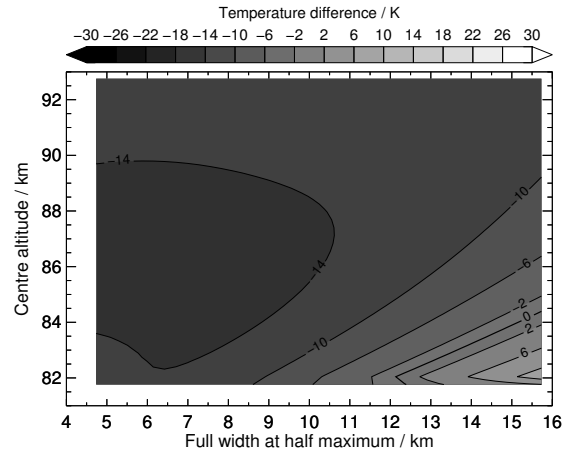

(a) Mean temperature difference between data measured by GRIPS 9 and the Na lidar at ALOMAR.

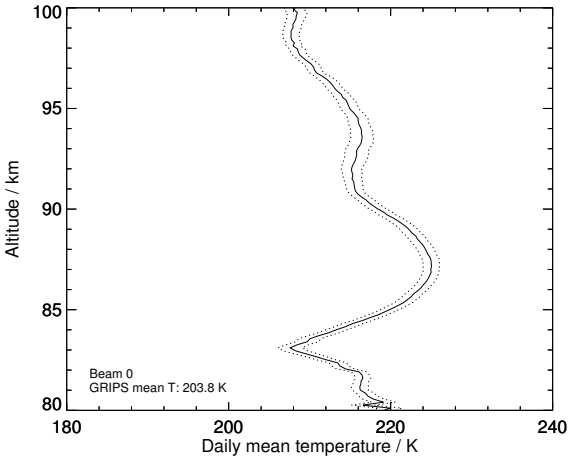

(b) Mean temperature profile from the beam with the best statistics which was used to compute panel (a).

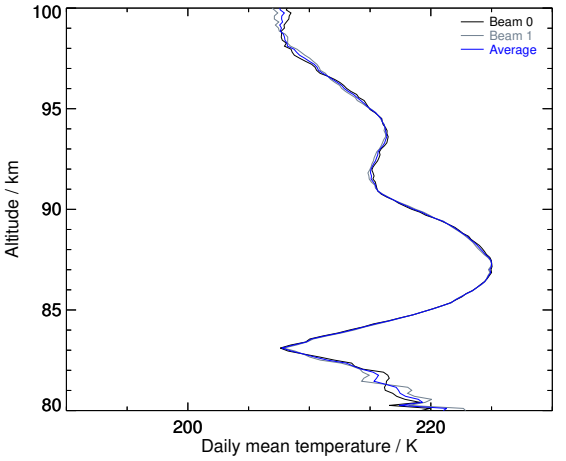

(c) Mean temperature profiles measured by the Na lidar's beam 0, beam 1, and the average of these.

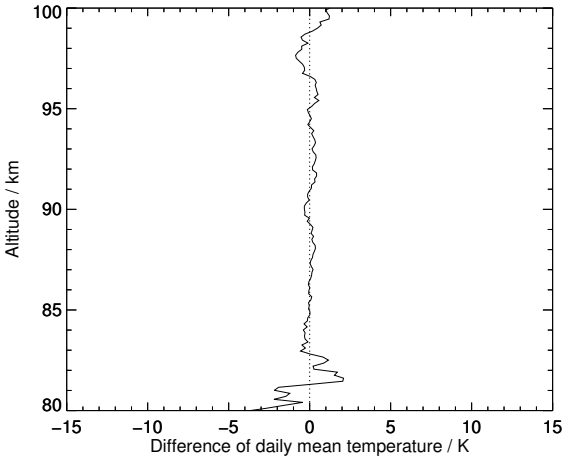

(d) Mean profile of the temperature difference between beam 0 and beam 1, shown in panel (c).

Figure S20: 2011–12–13

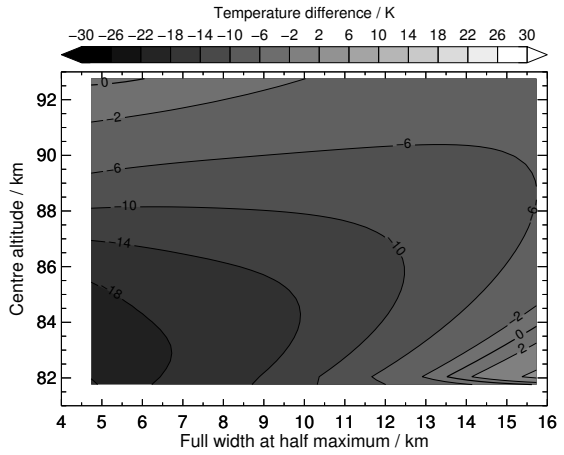

(a) Mean temperature difference between data measured by GRIPS 9 and the Na lidar at ALOMAR.

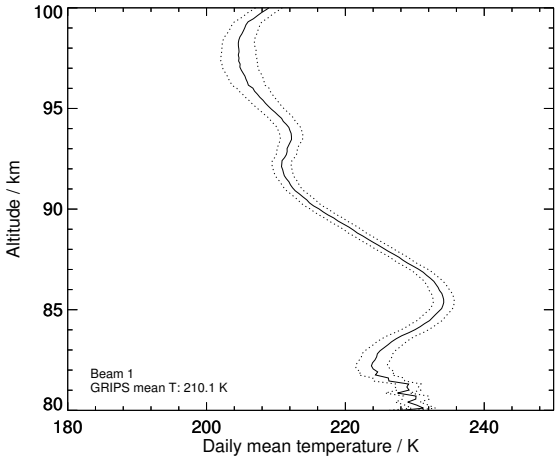

(b) Mean temperature profile from the beam with the best statistics which was used to compute panel (a).

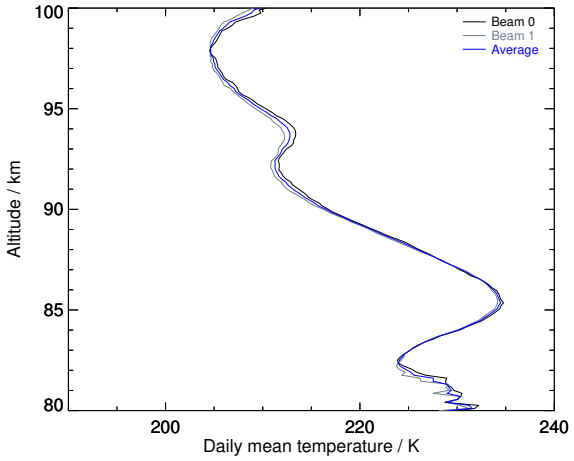

(c) Mean temperature profiles measured by the Na lidar's beam 0, beam 1, and the average of these.

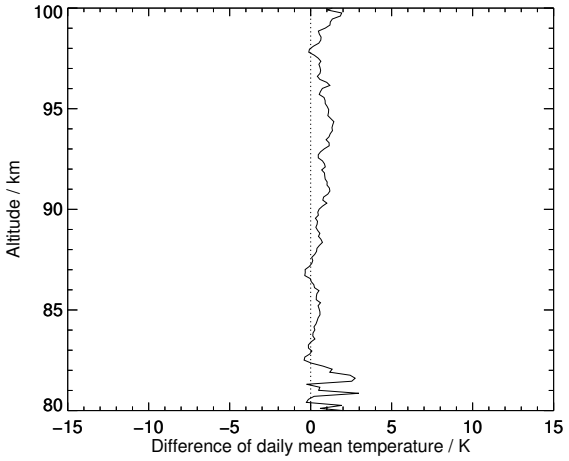

(d) Mean profile of the temperature difference between beam 0 and beam 1, shown in panel (c).

Figure S21: 2011–12–16

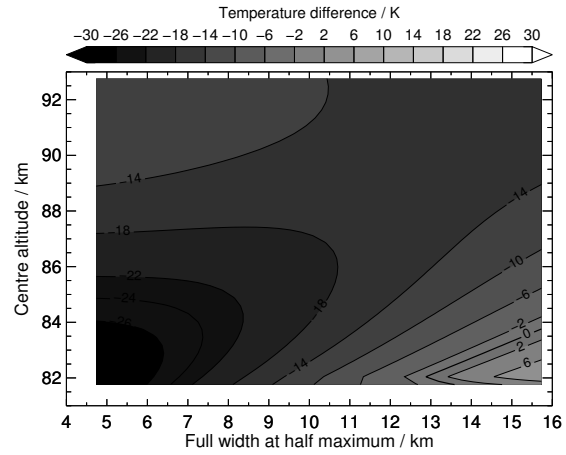

(a) Mean temperature difference between data measured by GRIPS 9 and the Na lidar at ALOMAR.

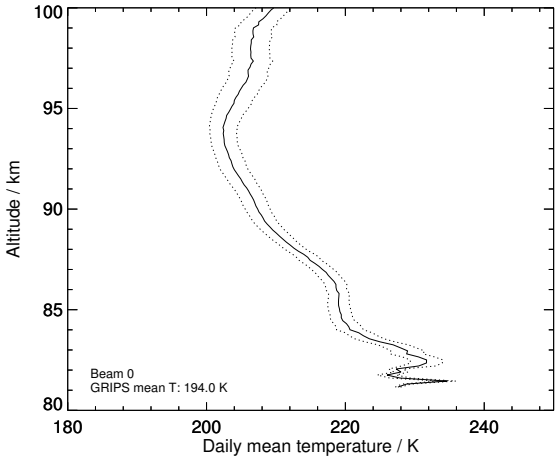

(b) Mean temperature profile from the beam with the best statistics which was used to compute panel (a).

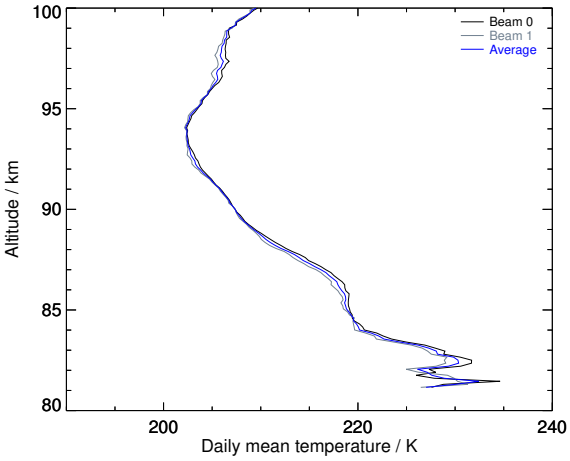

(c) Mean temperature profiles measured by the Na lidar's beam 0, beam 1, and the average of these.

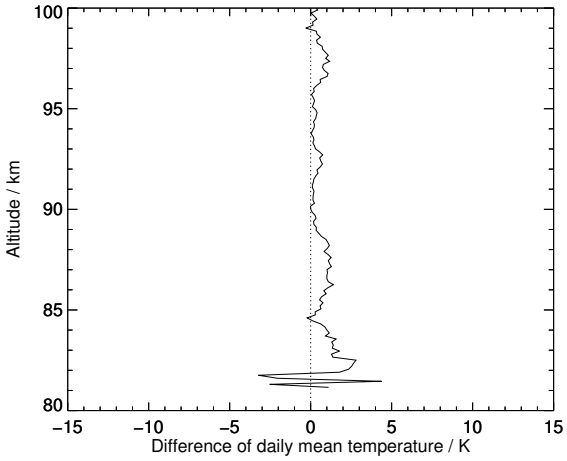

(d) Mean profile of the temperature difference between beam 0 and beam 1, shown in panel (c).

Figure S22: 2012–01–06

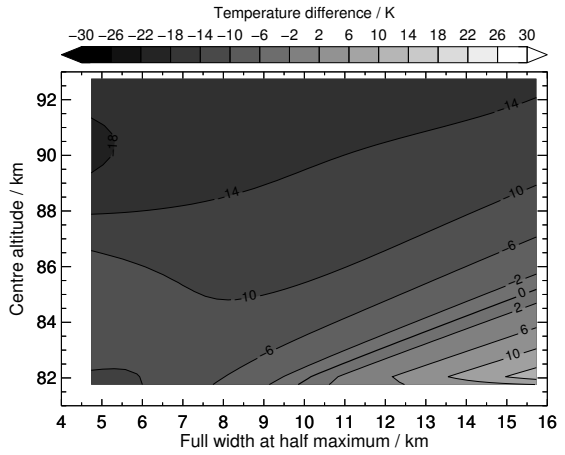

(a) Mean temperature difference between data measured by GRIPS 9 and the Na lidar at ALOMAR.

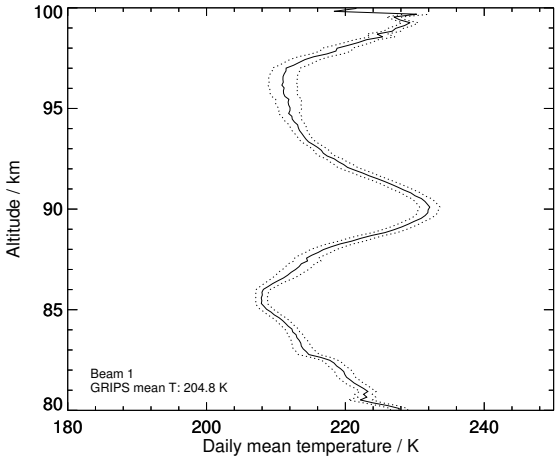

(b) Mean temperature profile from the beam with the best statistics which was used to compute panel (a).

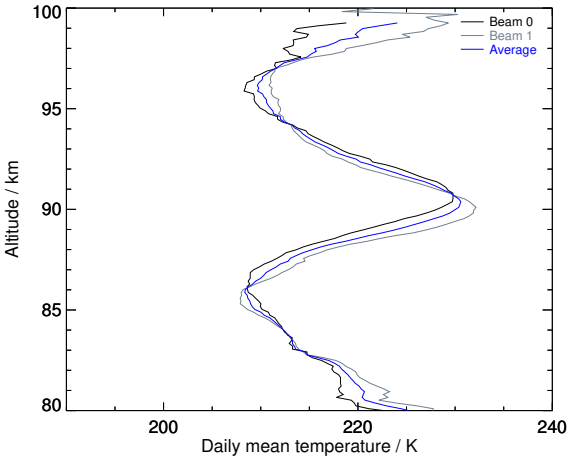

(c) Mean temperature profiles measured by the Na lidar's beam 0, beam 1, and the average of these.

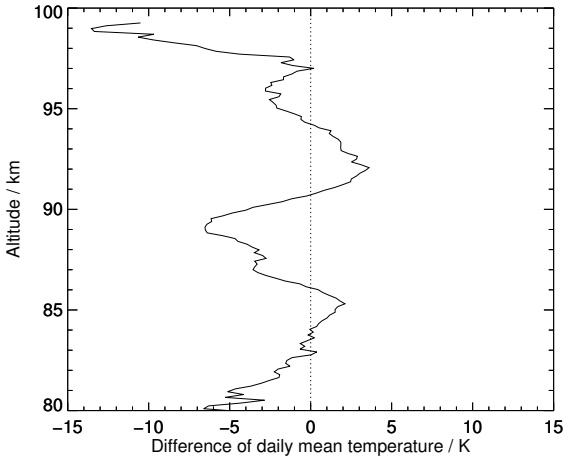

(d) Mean profile of the temperature difference between beam 0 and beam 1, shown in panel (c).

Figure S23: 2012–01–19

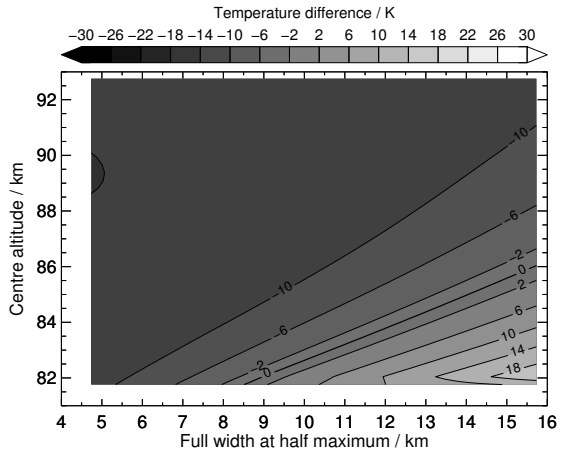

(a) Mean temperature difference between data measured by GRIPS 9 and the Na lidar at ALOMAR.

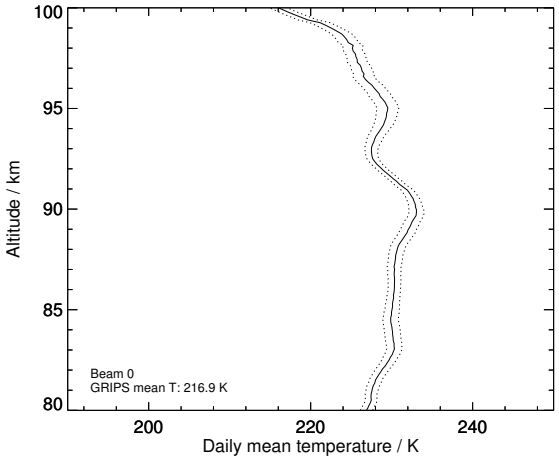

(b) Mean temperature profile from the beam with the best statistics which was used to compute panel (a).

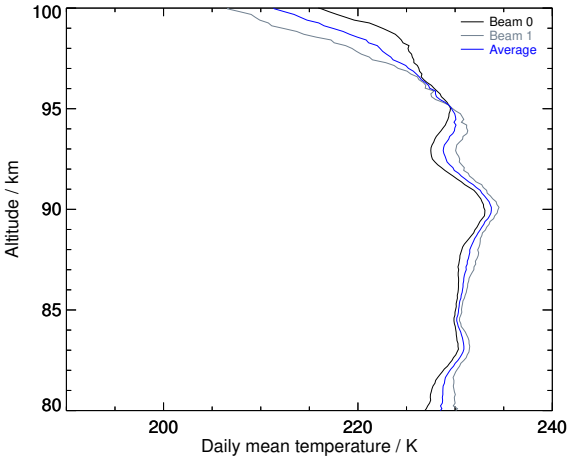

(c) Mean temperature profiles measured by the Na lidar's beam 0, beam 1, and the average of these.

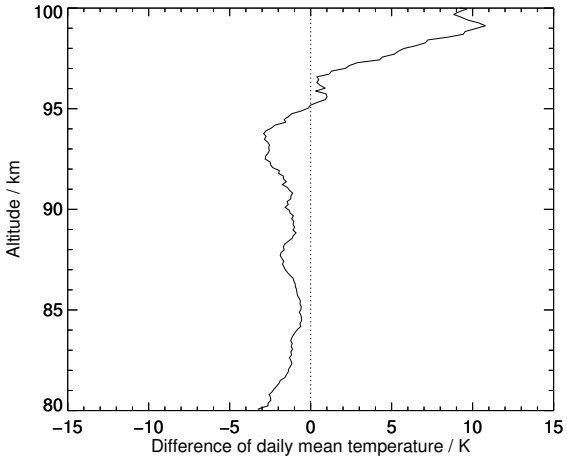

(d) Mean profile of the temperature difference between beam 0 and beam 1, shown in panel (c).

Figure S24: 2012–01–21

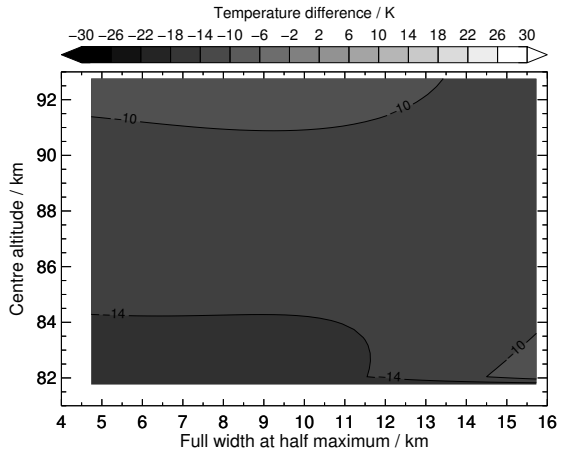

(a) Mean temperature difference between data measured by GRIPS 9 and the Na lidar at ALOMAR.

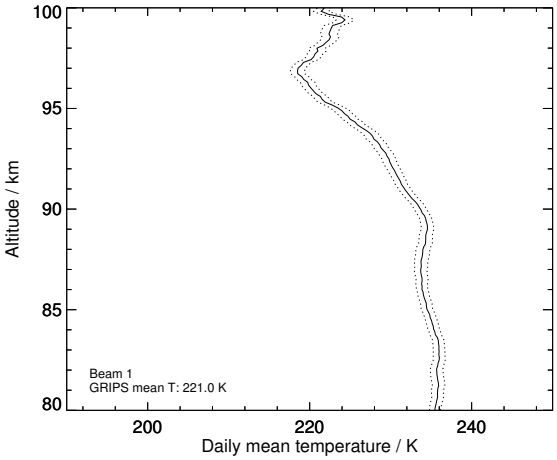

(b) Mean temperature profile from the beam with the best statistics which was used to compute panel (a).

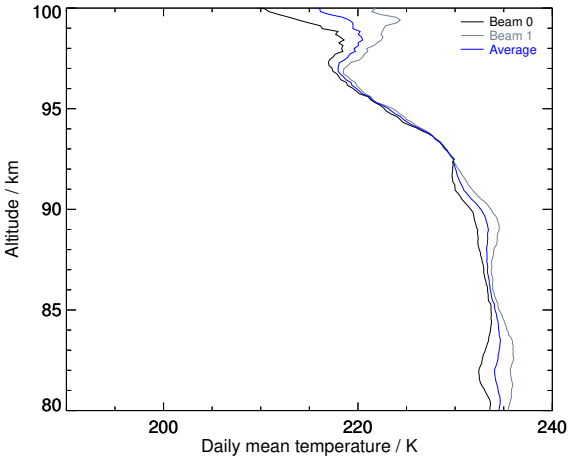

(c) Mean temperature profiles measured by the Na lidar's beam 0, beam 1, and the average of these.

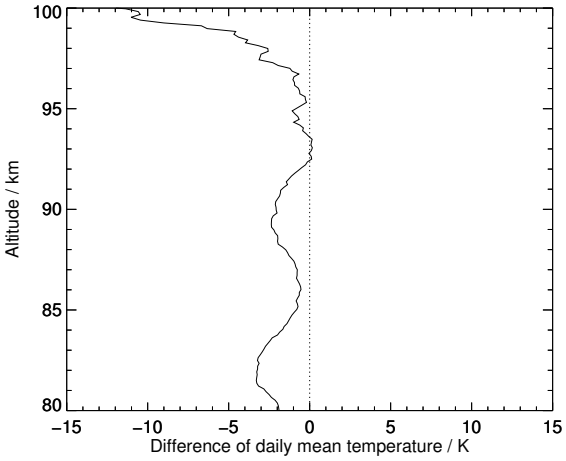

(d) Mean profile of the temperature difference between beam 0 and beam 1, shown in panel (c).

Figure S25: 2012–01–22

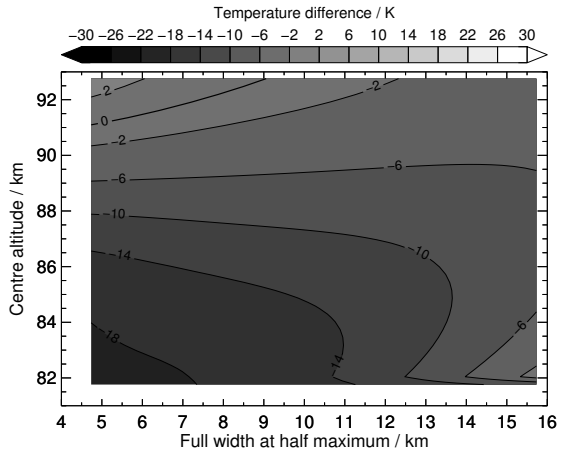

(a) Mean temperature difference between data measured by GRIPS 9 and the Na lidar at ALOMAR.

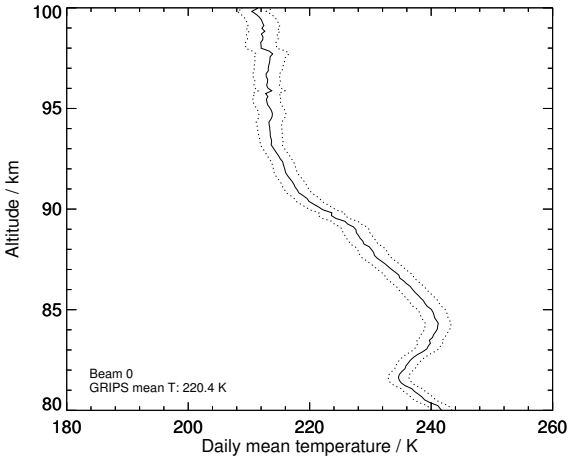

(b) Mean temperature profile from the beam with the best statistics which was used to compute panel (a).

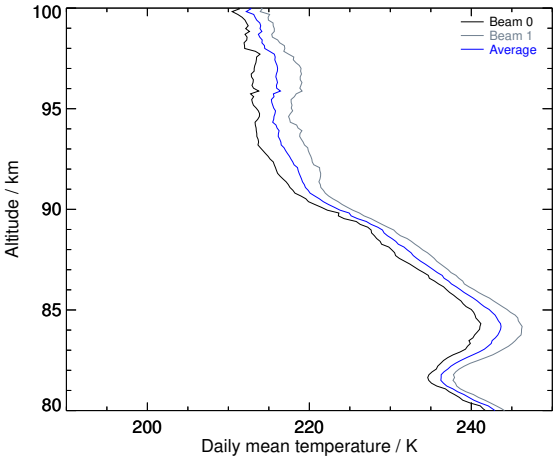

(c) Mean temperature profiles measured by the Na lidar's beam 0, beam 1, and the average of these.

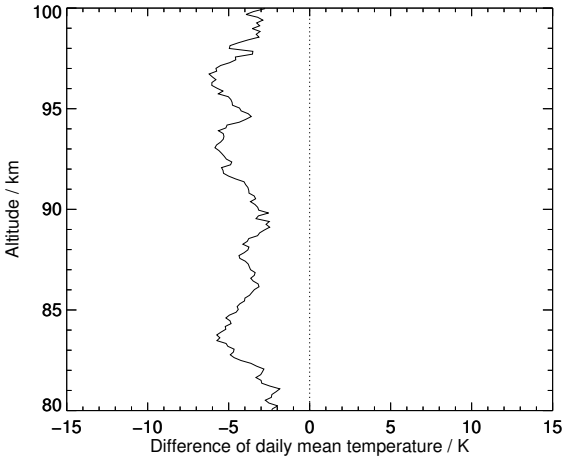

(d) Mean profile of the temperature difference between beam 0 and beam 1, shown in panel (c).

Figure S26: 2012–01–24

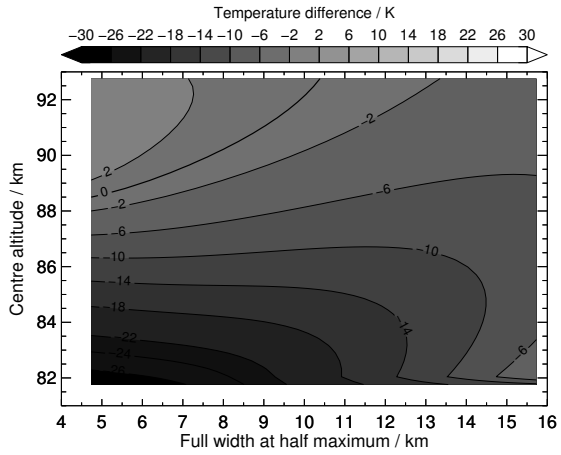

(a) Mean temperature difference between data measured by GRIPS 9 and the Na lidar at ALOMAR.

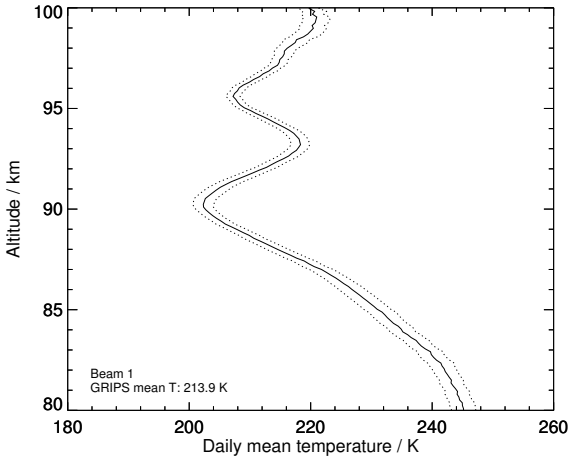

(b) Mean temperature profile from the beam with the best statistics which was used to compute panel (a).

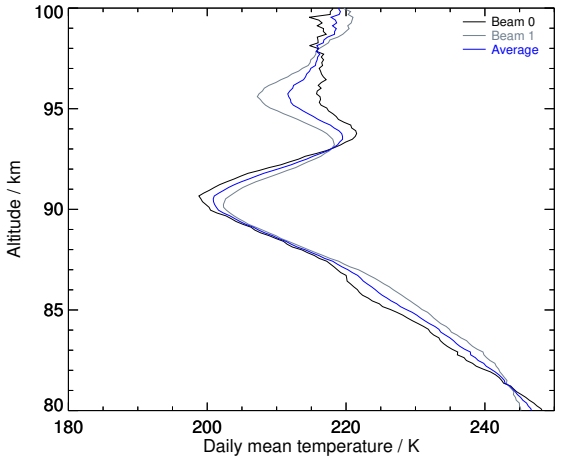

(c) Mean temperature profiles measured by the Na lidar's beam 0, beam 1, and the average of these.

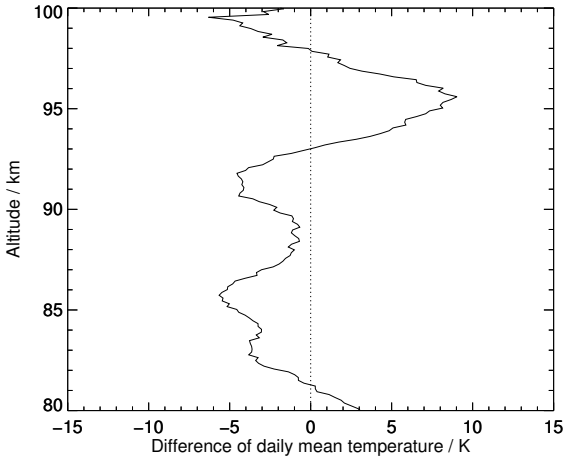

(d) Mean profile of the temperature difference between beam 0 and beam 1, shown in panel (c).

Figure S27: 2012–02–01

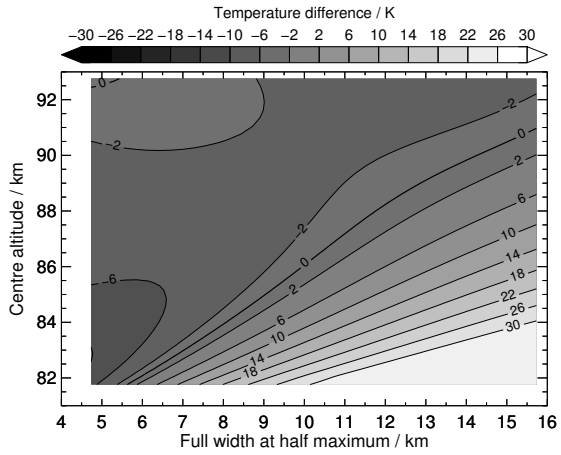

(a) Mean temperature difference between data measured by GRIPS 9 and the Na lidar at ALOMAR.

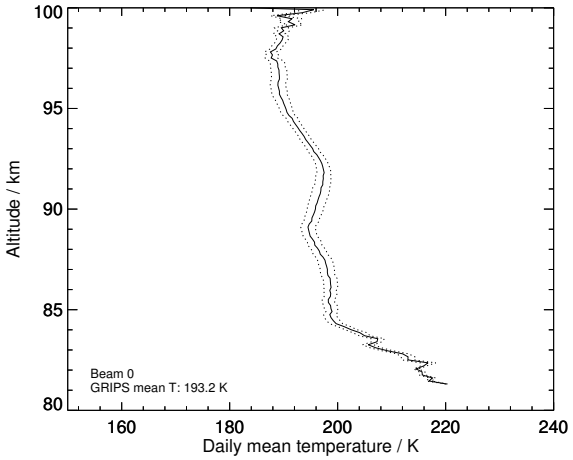

(b) Mean temperature profile from the beam with the best statistics which was used to compute panel (a).

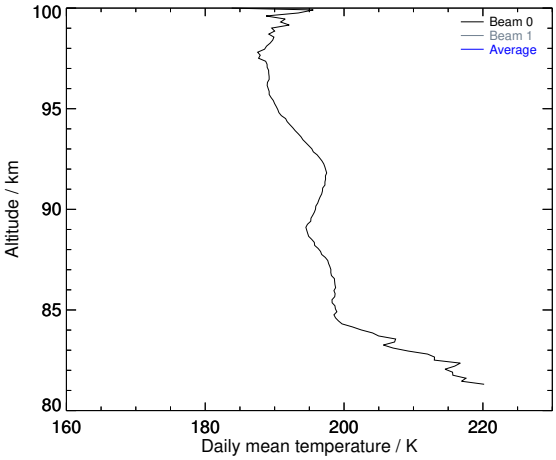

(c) Mean temperature profiles measured by the Na lidar's beam 0, beam 1, and the average of these.

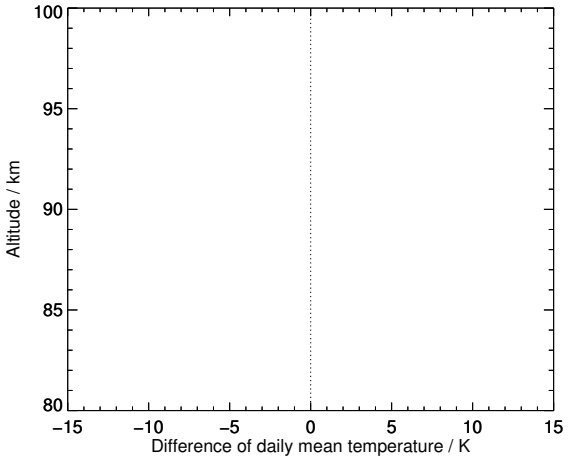

(d) Mean profile of the temperature difference between beam 0 and beam 1, shown in panel (c).

Figure S28: 2012–03–20

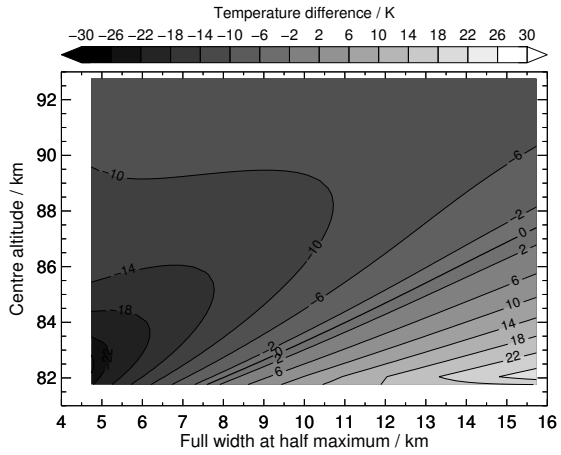

(a) Mean temperature difference between data measured by GRIPS 9 and the Na lidar at ALOMAR.

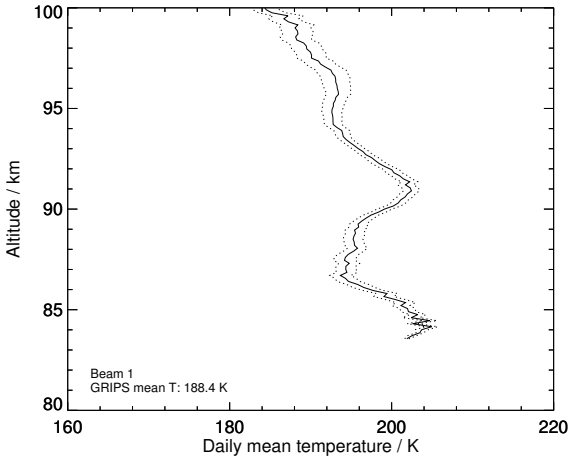

(b) Mean temperature profile from the beam with the best statistics which was used to compute panel (a).

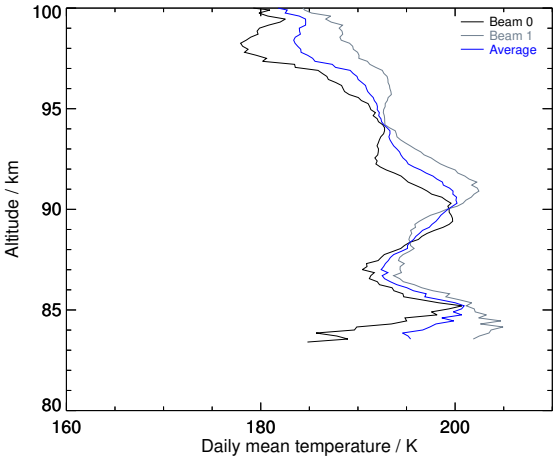

(c) Mean temperature profiles measured by the Na lidar's beam 0, beam 1, and the average of these.

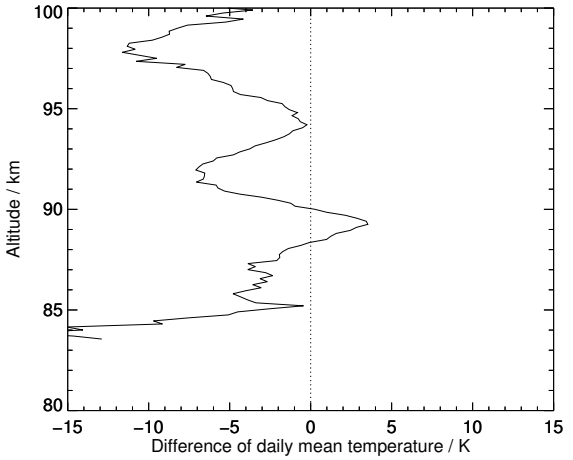

(d) Mean profile of the temperature difference between beam 0 and beam 1, shown in panel (c).

Figure S29: 2013–04–13

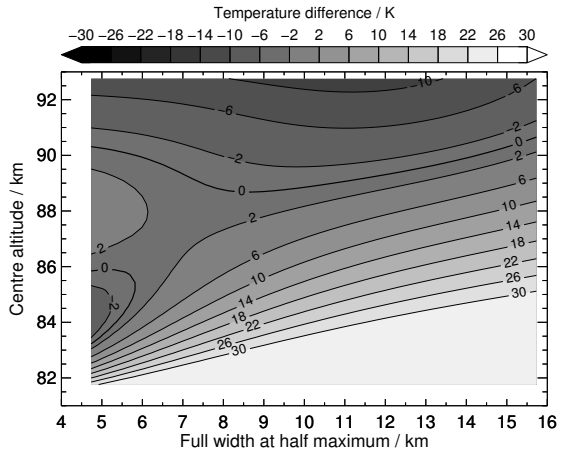

(a) Mean temperature difference between data measured by GRIPS 9 and the Na lidar at ALOMAR.

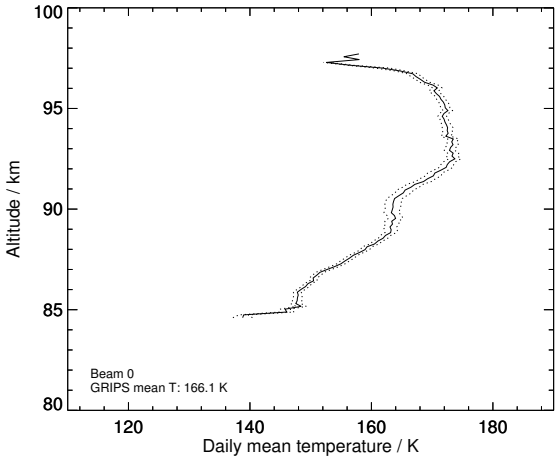

(b) Mean temperature profile from the beam with the best statistics which was used to compute panel (a).

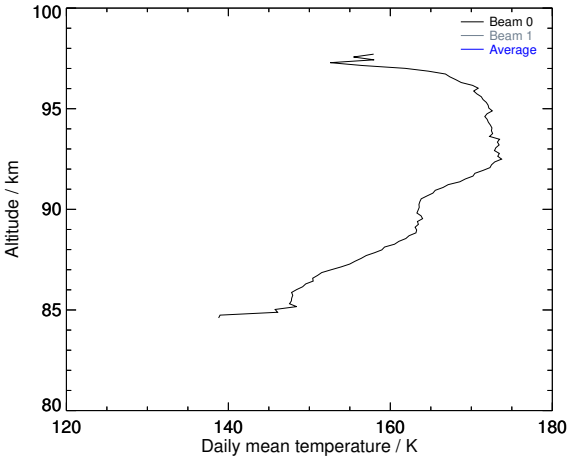

(c) Mean temperature profiles measured by the Na lidar's beam 0, beam 1, and the average of these.

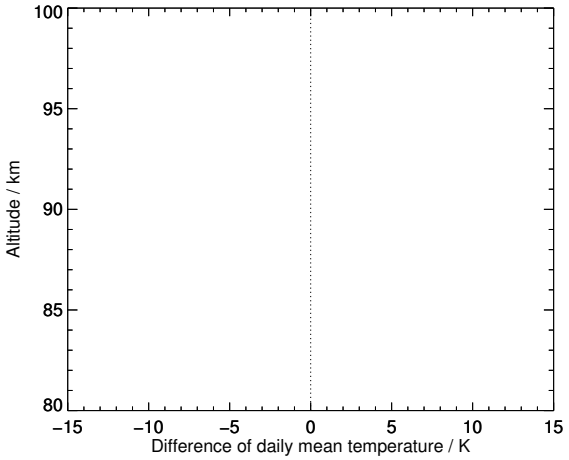

(d) Mean profile of the temperature difference between beam 0 and beam 1, shown in panel (c).

Figure S30: 2013–09–02

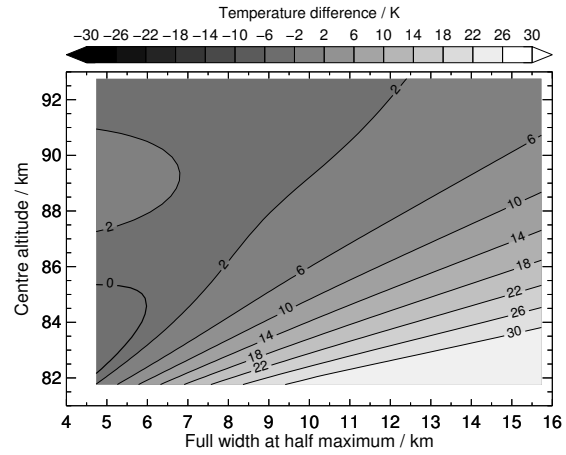

(a) Mean temperature difference between data measured by GRIPS 9 and the Na lidar at ALOMAR.

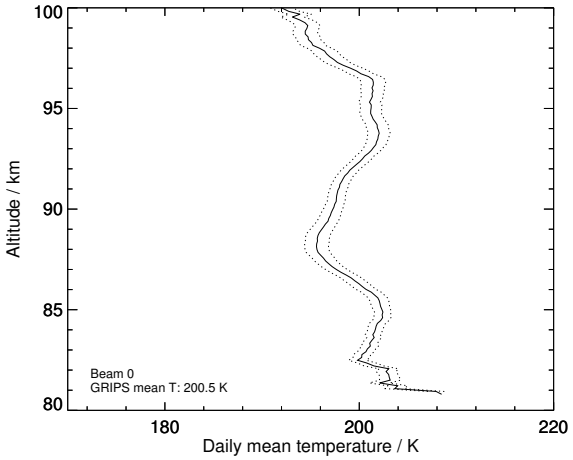

(b) Mean temperature profile from the beam with the best statistics which was used to compute panel (a).

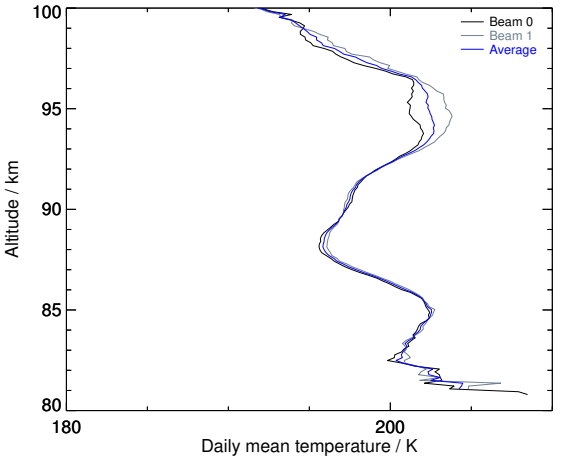

(c) Mean temperature profiles measured by the Na lidar's beam 0, beam 1, and the average of these.

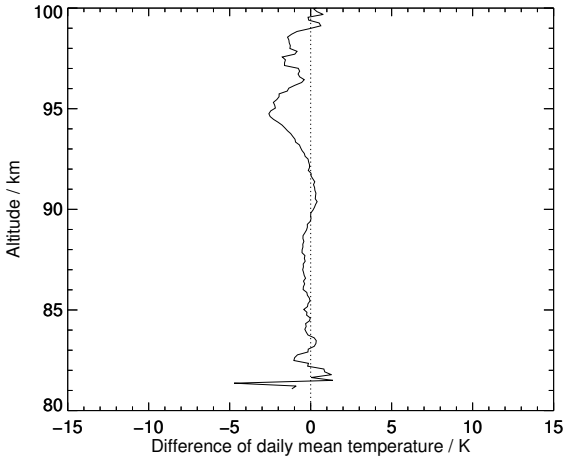

(d) Mean profile of the temperature difference between beam 0 and beam 1, shown in panel (c).

Figure S31: 2013–09–18

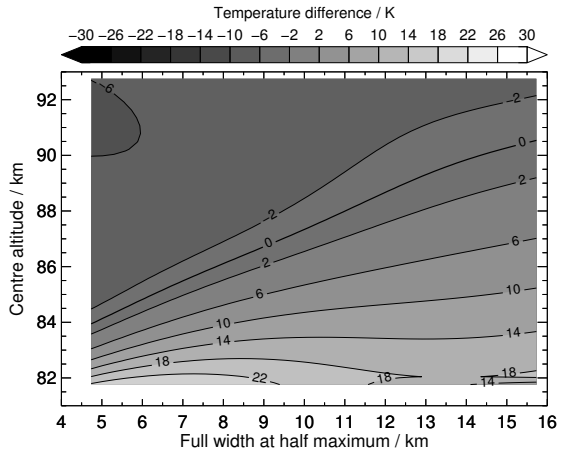

(a) Mean temperature difference between data measured by GRIPS 9 and the Na lidar at ALOMAR.

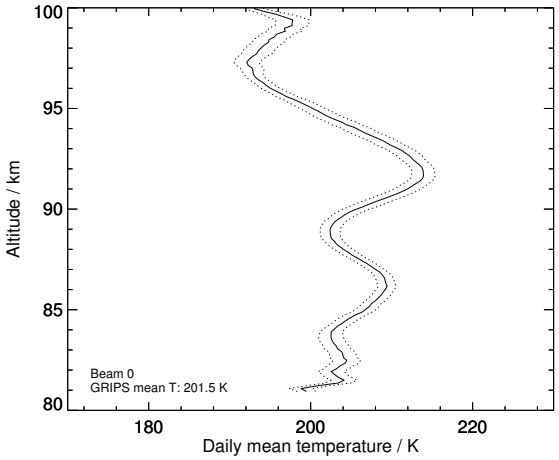

(b) Mean temperature profile from the beam with the best statistics which was used to compute panel (a).

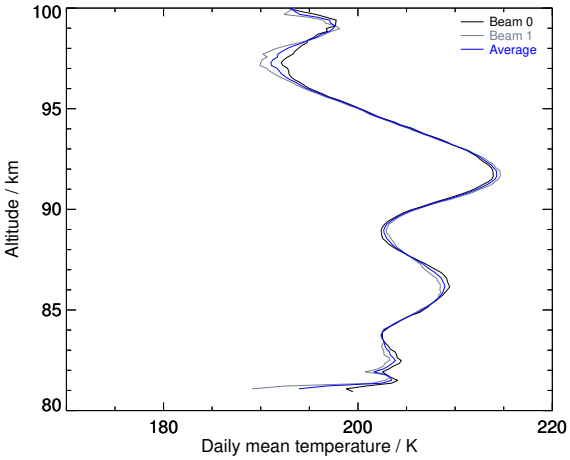

(c) Mean temperature profiles measured by the Na lidar's beam 0, beam 1, and the average of these.

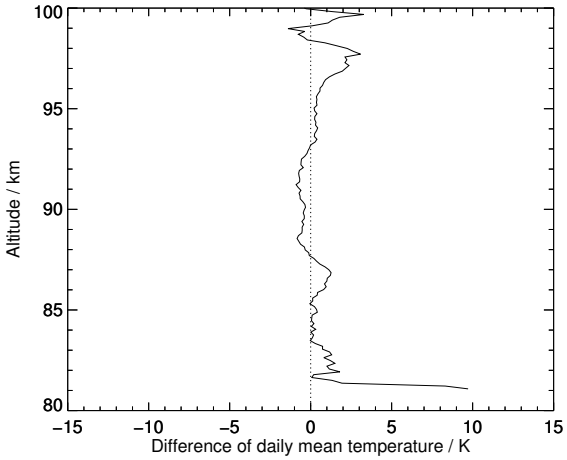

(d) Mean profile of the temperature difference between beam 0 and beam 1, shown in panel (c).

Figure S32: 2013–09–23

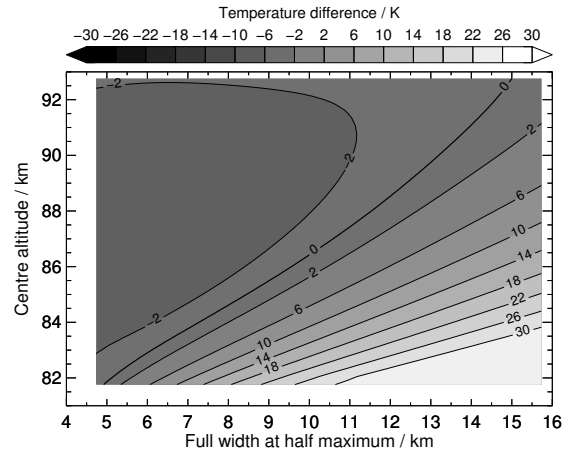

(a) Mean temperature difference between data measured by GRIPS 9 and the Na lidar at ALOMAR.

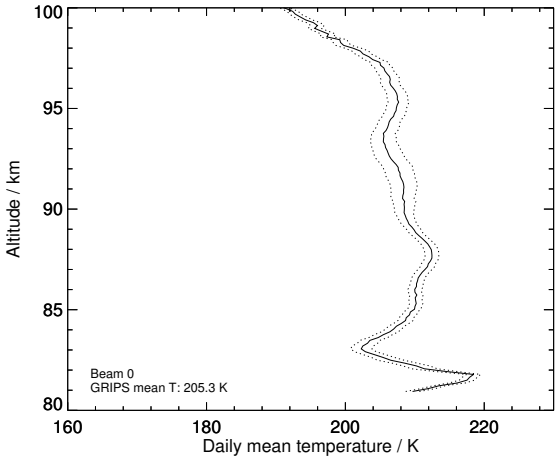

(b) Mean temperature profile from the beam with the best statistics which was used to compute panel (a).

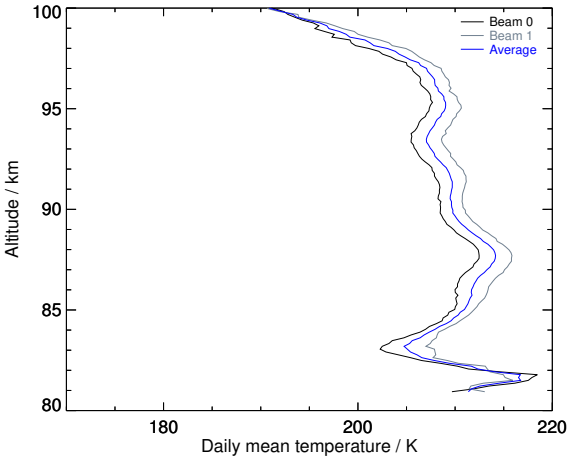

(c) Mean temperature profiles measured by the Na lidar's beam 0, beam 1, and the average of these.

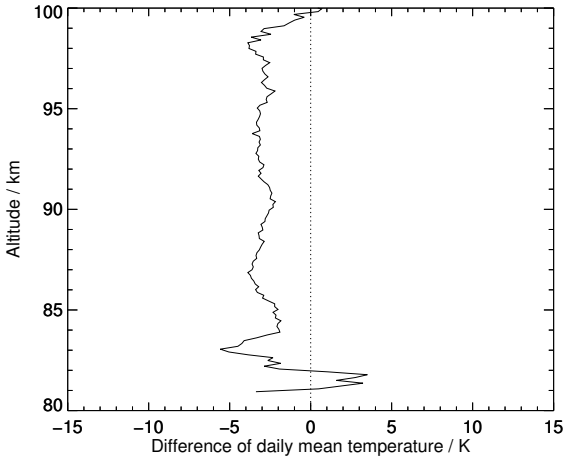

(d) Mean profile of the temperature difference between beam 0 and beam 1, shown in panel (c).

Figure S33: 2013–09–24

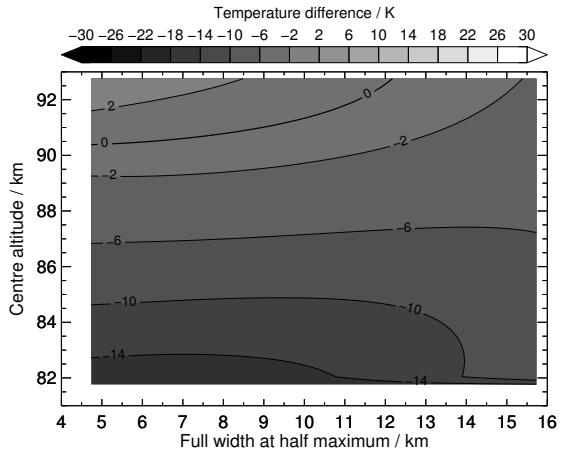

(a) Mean temperature difference between data measured by GRIPS 9 and the Na lidar at ALOMAR.

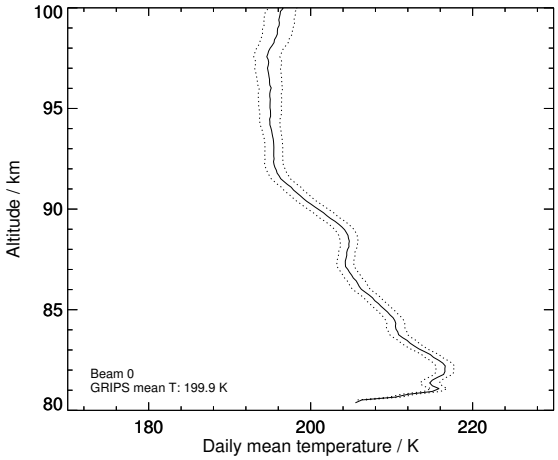

(b) Mean temperature profile from the beam with the best statistics which was used to compute panel (a).

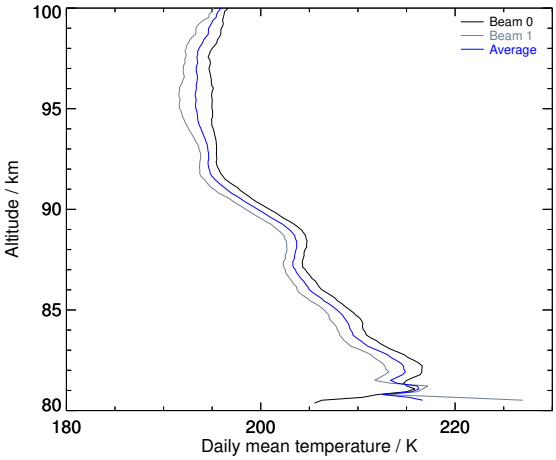

(c) Mean temperature profiles measured by the Na lidar's beam 0, beam 1, and the average of these.

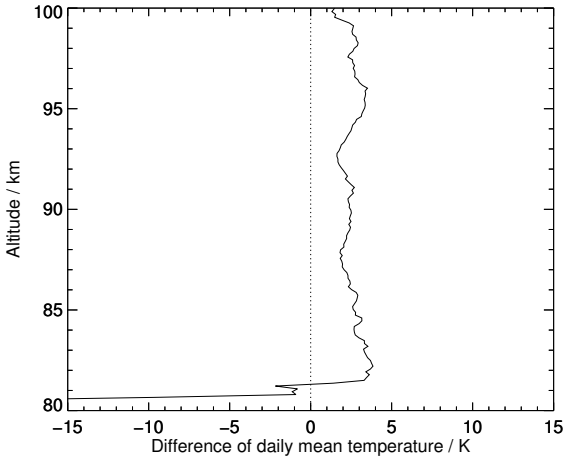

(d) Mean profile of the temperature difference between beam 0 and beam 1, shown in panel (c).

Figure S34: 2013–09–27

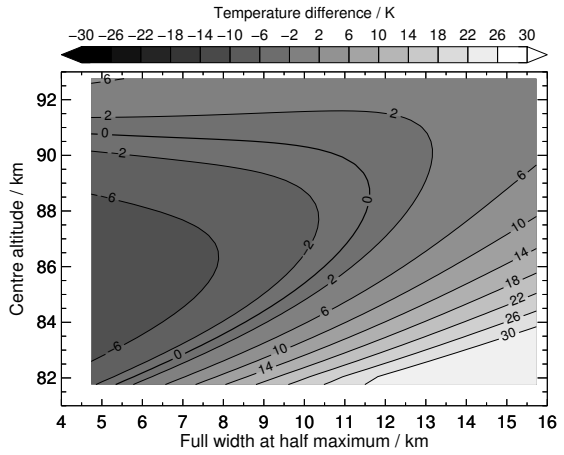

(a) Mean temperature difference between data measured by GRIPS 9 and the Na lidar at ALOMAR.

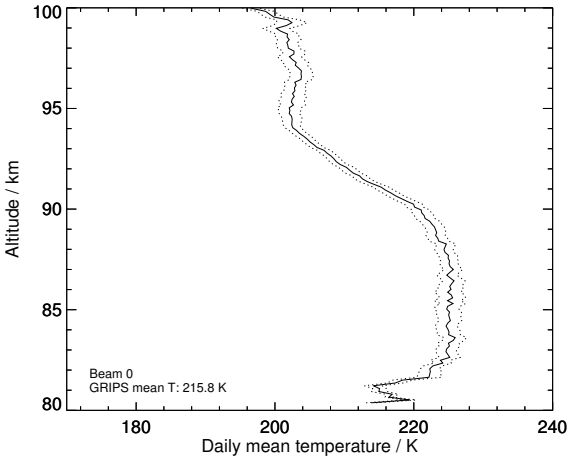

(b) Mean temperature profile from the beam with the best statistics which was used to compute panel (a).

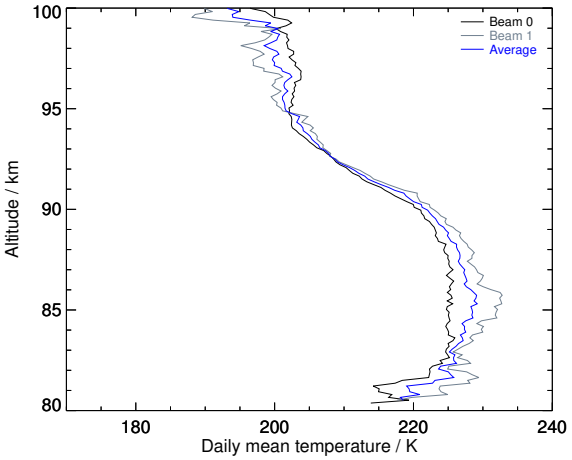

(c) Mean temperature profiles measured by the Na lidar's beam 0, beam 1, and the average of these.

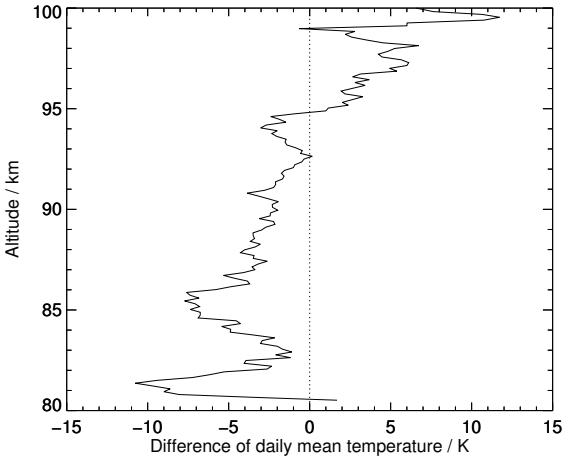

(d) Mean profile of the temperature difference between beam 0 and beam 1, shown in panel (c).

Figure S35: 2013–11–08

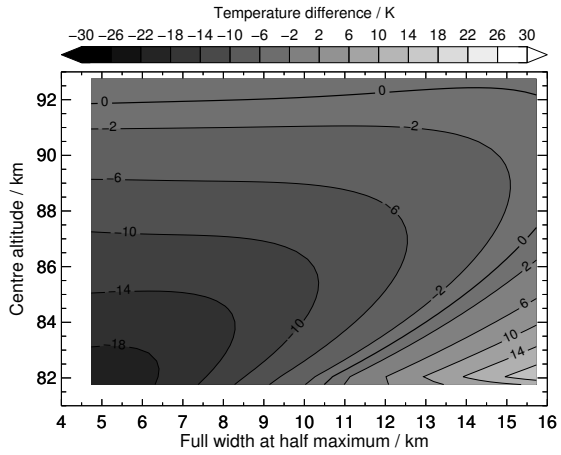

(a) Mean temperature difference between data measured by GRIPS 9 and the Na lidar at ALOMAR.

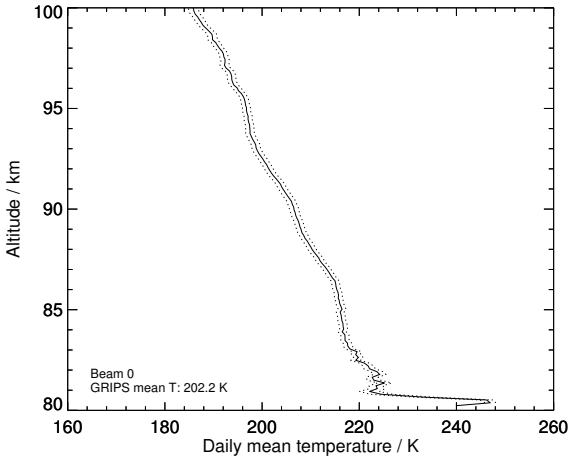

(b) Mean temperature profile from the beam with the best statistics which was used to compute panel (a).

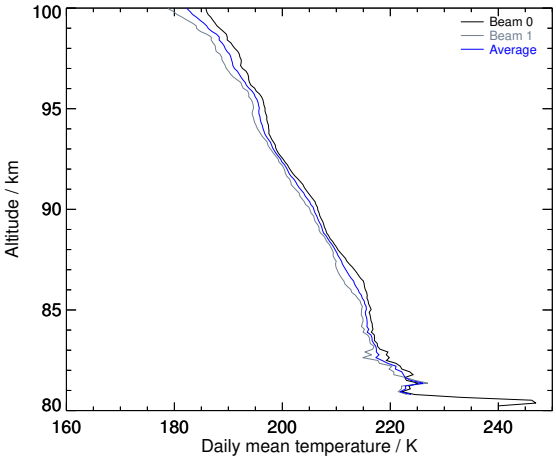

(c) Mean temperature profiles measured by the Na lidar's beam 0, beam 1, and the average of these.

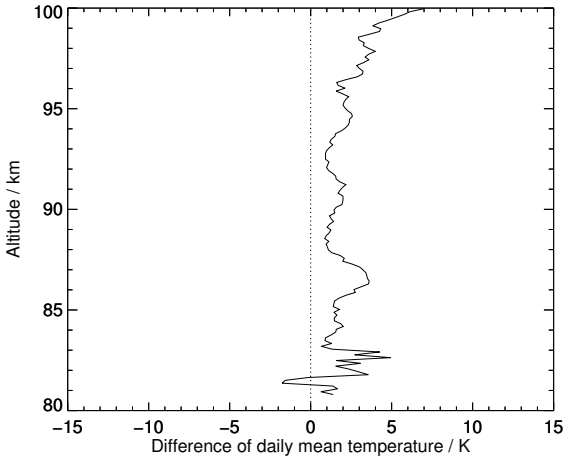

(d) Mean profile of the temperature difference between beam 0 and beam 1, shown in panel (c).

Figure S36: 2013–12–06

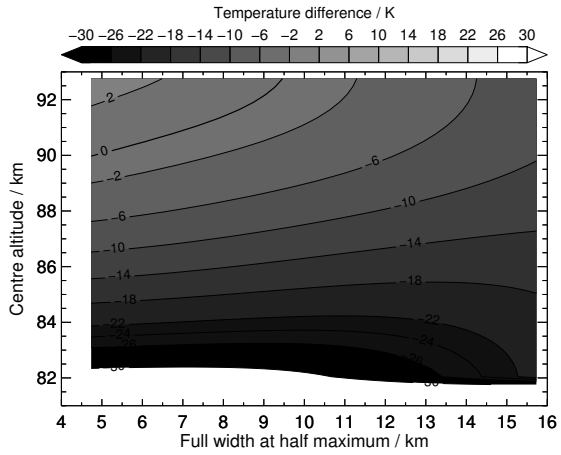

(a) Mean temperature difference between data measured by GRIPS 9 and the Na lidar at ALOMAR.

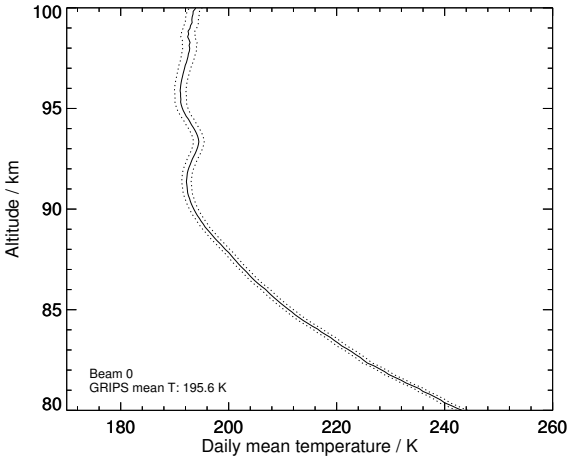

(b) Mean temperature profile from the beam with the best statistics which was used to compute panel (a).

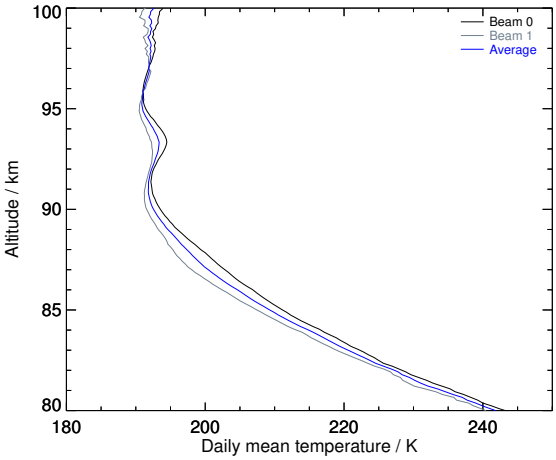

(c) Mean temperature profiles measured by the Na lidar's beam 0, beam 1, and the average of these.

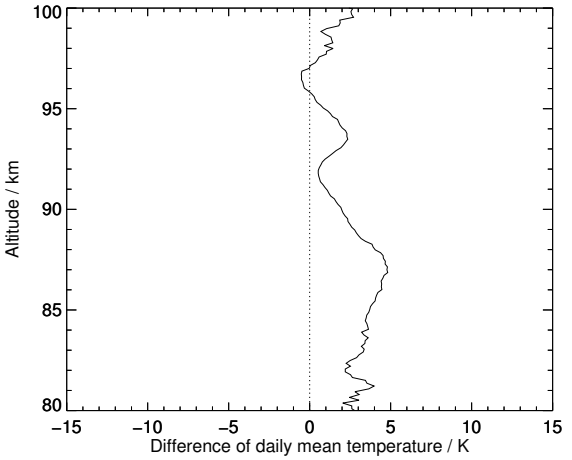

(d) Mean profile of the temperature difference between beam 0 and beam 1, shown in panel (c).

Figure S37: 2013–12–08

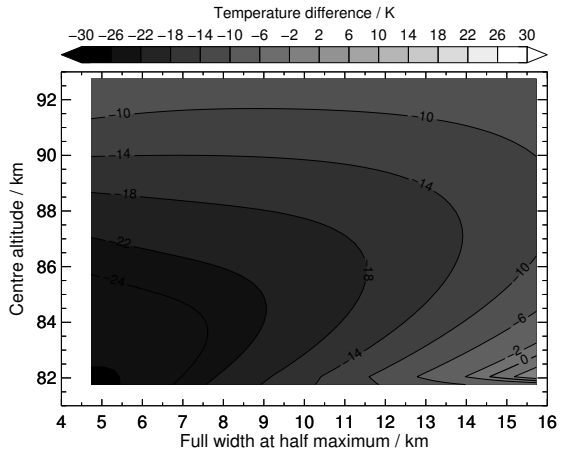

(a) Mean temperature difference between data measured by GRIPS 9 and the Na lidar at ALOMAR.

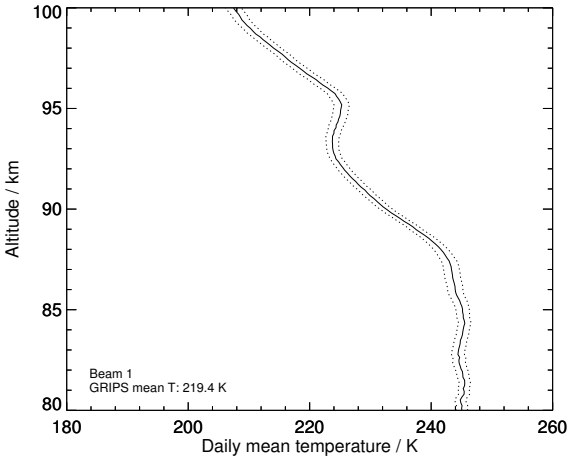

(b) Mean temperature profile from the beam with the best statistics which was used to compute panel (a).

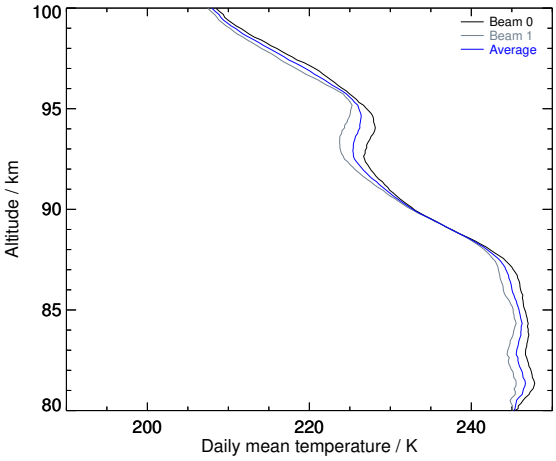

(c) Mean temperature profiles measured by the Na lidar's beam 0, beam 1, and the average of these.

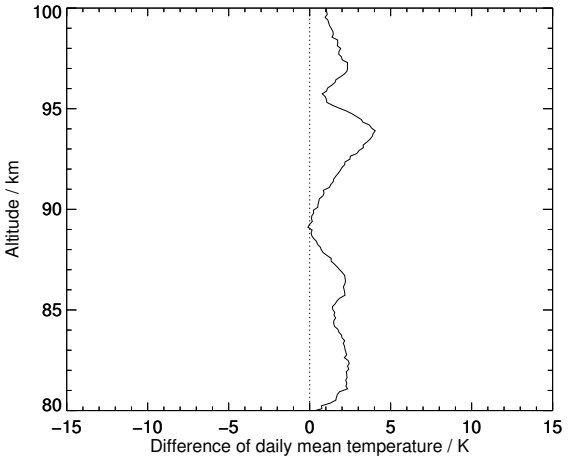

(d) Mean profile of the temperature difference between beam 0 and beam 1, shown in panel (c).

Figure S38: 2014–01–10

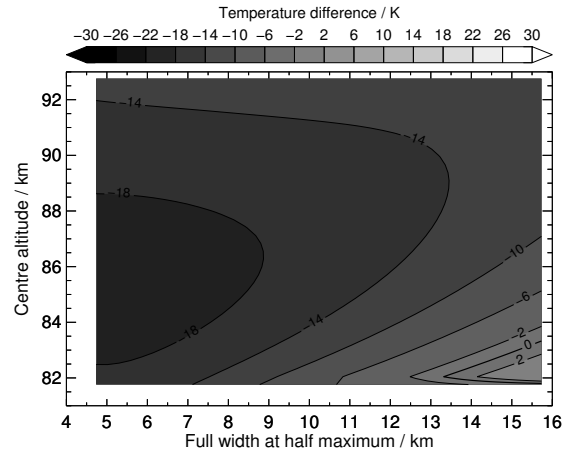

(a) Mean temperature difference between data measured by GRIPS 9 and the Na lidar at ALOMAR.

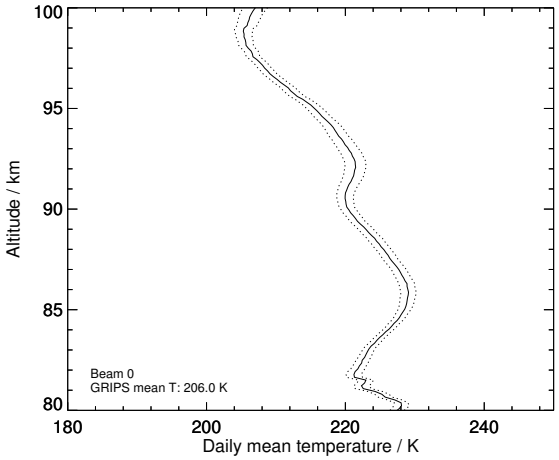

(b) Mean temperature profile from the beam with the best statistics which was used to compute panel (a).

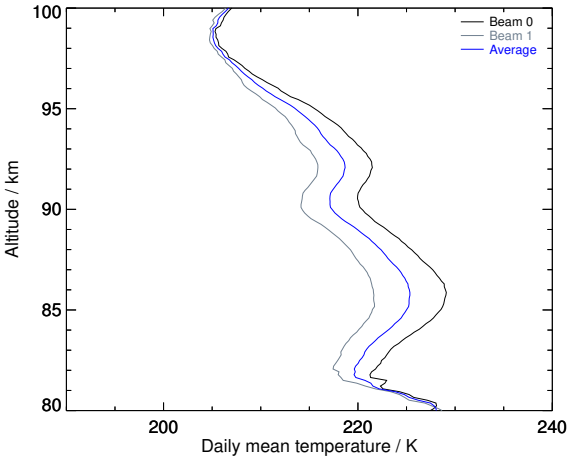

(c) Mean temperature profiles measured by the Na lidar's beam 0, beam 1, and the average of these.

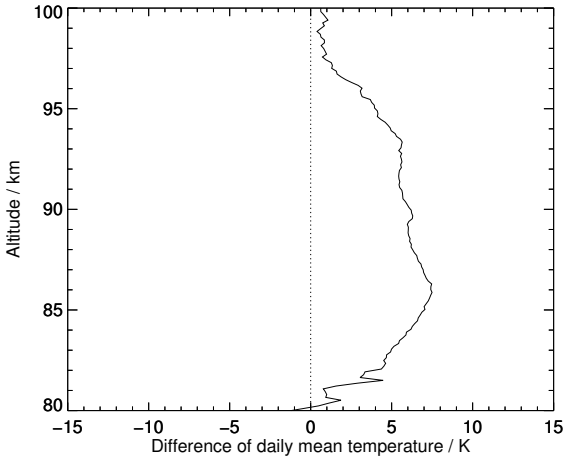

(d) Mean profile of the temperature difference between beam 0 and beam 1, shown in panel (c).

Figure S39: 2014–01–15

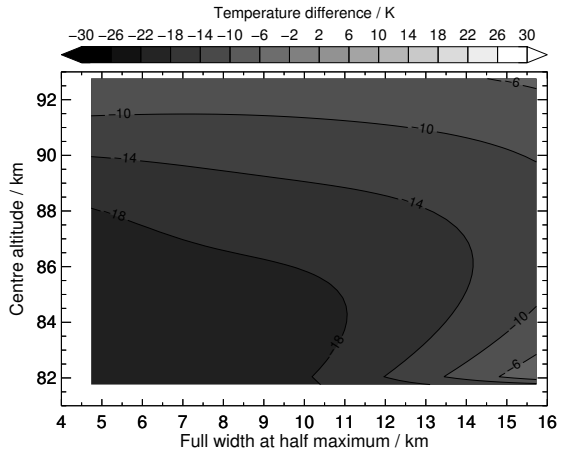

(a) Mean temperature difference between data measured by GRIPS 9 and the Na lidar at ALOMAR.

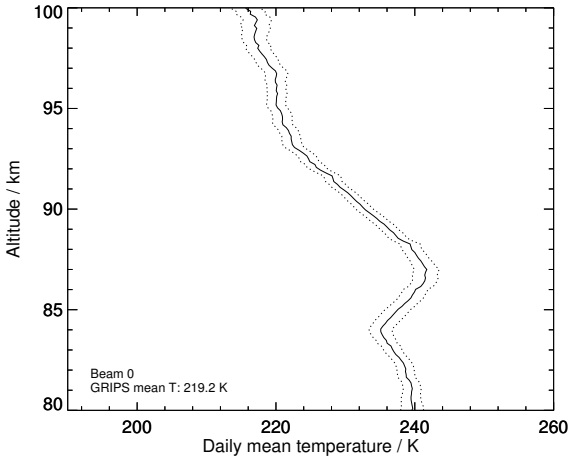

(b) Mean temperature profile from the beam with the best statistics which was used to compute panel (a).

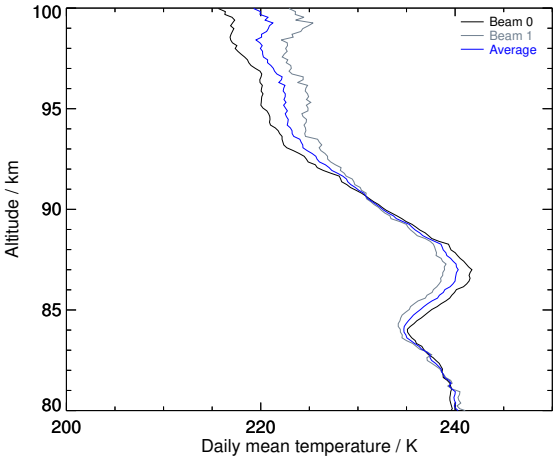

(c) Mean temperature profiles measured by the Na lidar's beam 0, beam 1, and the average of these.

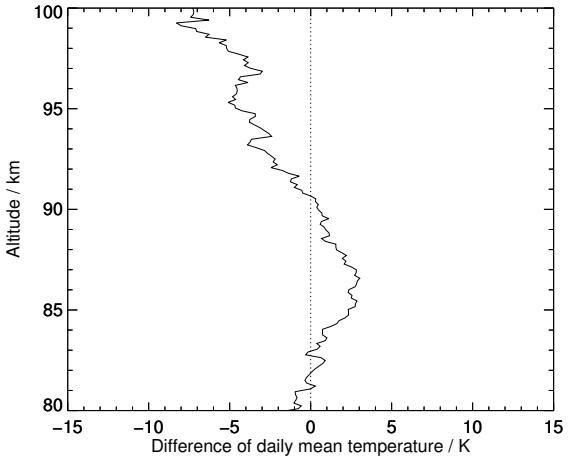

(d) Mean profile of the temperature difference between beam 0 and beam 1, shown in panel (c).

Figure S40: 2014–01–21

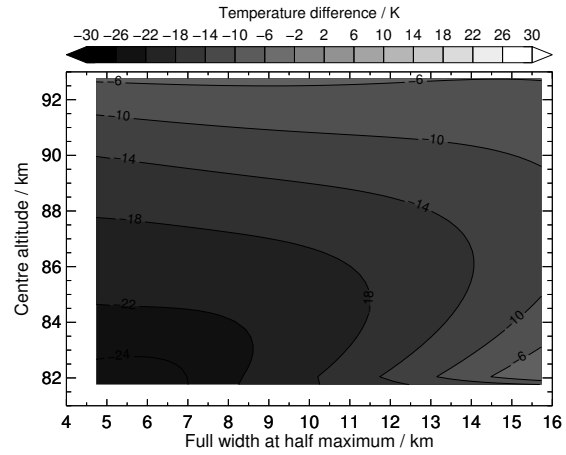

(a) Mean temperature difference between data measured by GRIPS 9 and the Na lidar at ALOMAR.

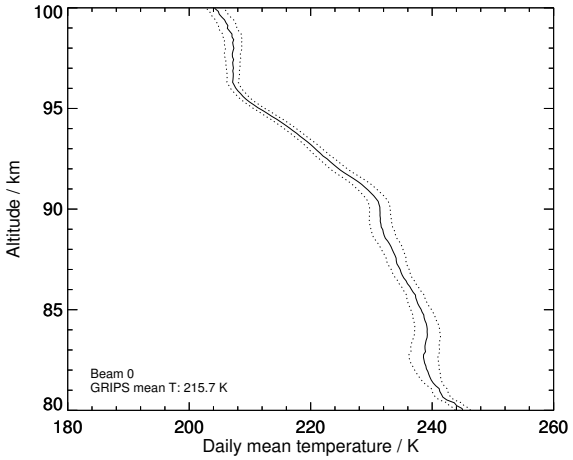

(b) Mean temperature profile from the beam with the best statistics which was used to compute panel (a).

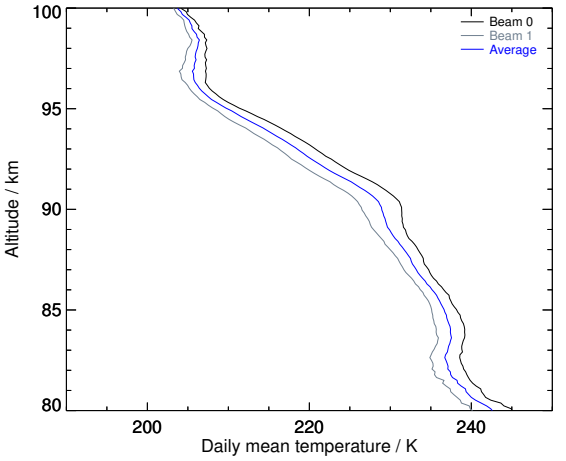

(c) Mean temperature profiles measured by the Na lidar's beam 0, beam 1, and the average of these.

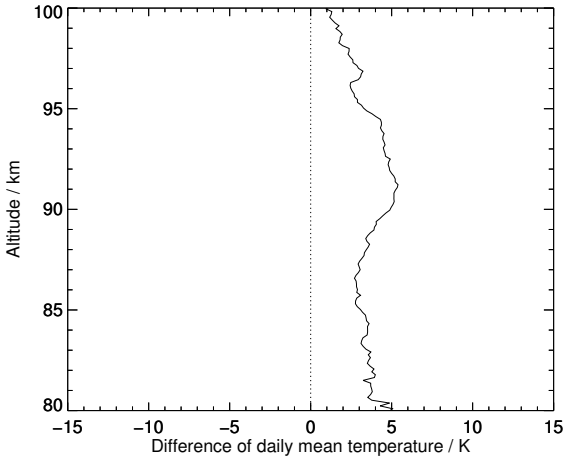

(d) Mean profile of the temperature difference between beam 0 and beam 1, shown in panel (c).

Figure S41: 2014–01–22

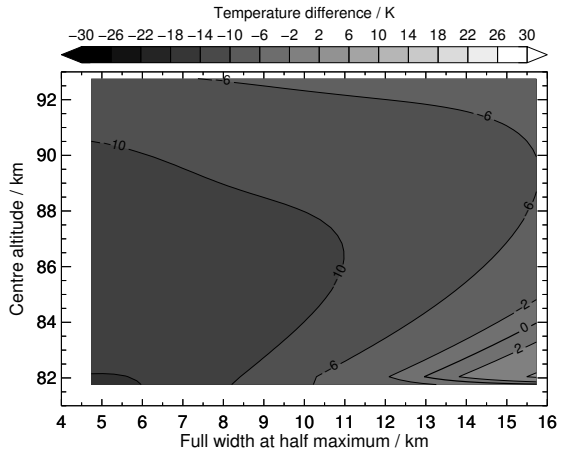

(a) Mean temperature difference between data measured by GRIPS 9 and the Na lidar at ALOMAR.

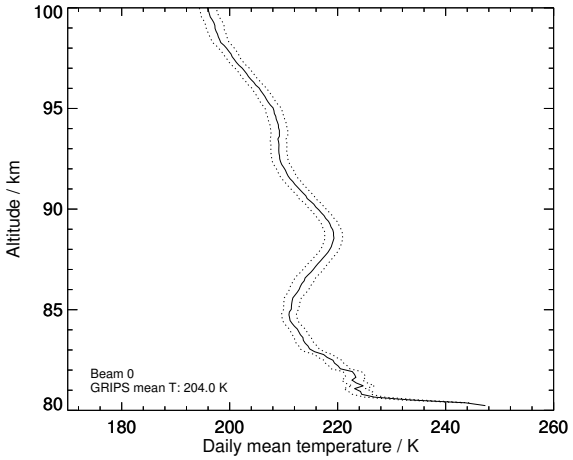

(b) Mean temperature profile from the beam with the best statistics which was used to compute panel (a).

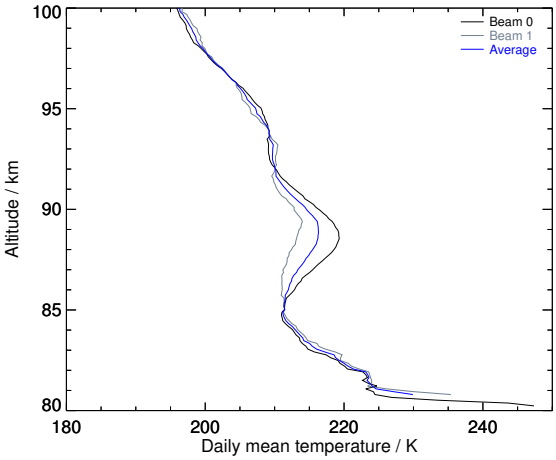

(c) Mean temperature profiles measured by the Na lidar's beam 0, beam 1, and the average of these.

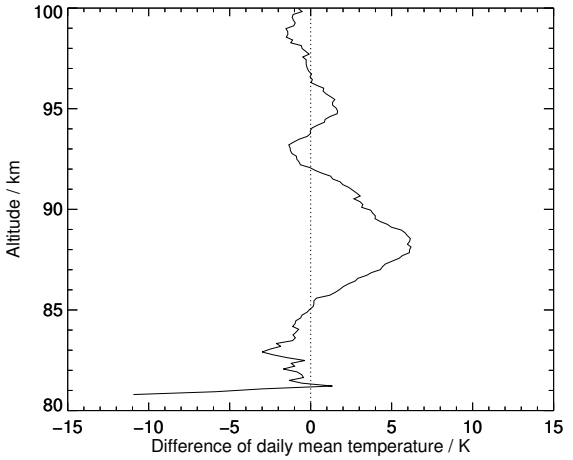

(d) Mean profile of the temperature difference between beam 0 and beam 1, shown in panel (c).

Figure S42: 2014–01–24

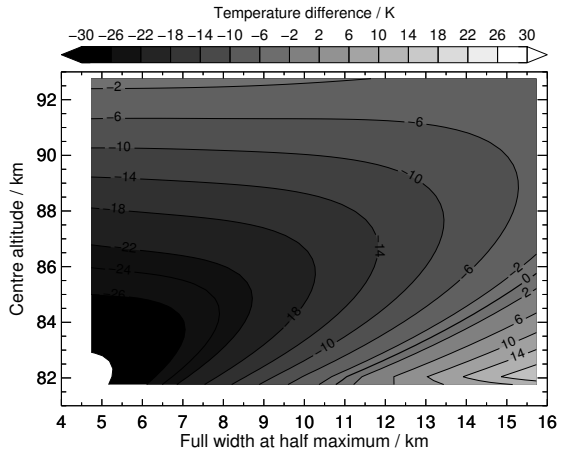

(a) Mean temperature difference between data measured by GRIPS 9 and the Na lidar at ALOMAR.

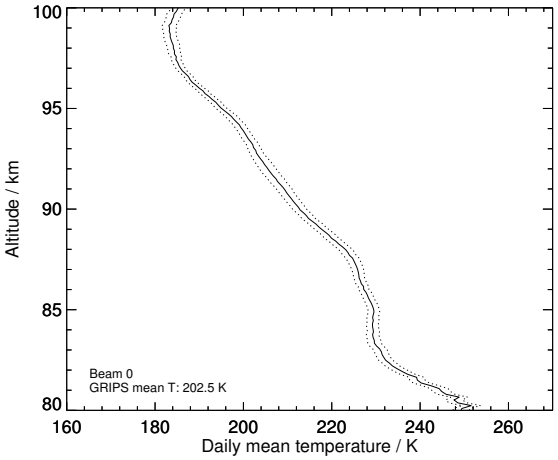

(b) Mean temperature profile from the beam with the best statistics which was used to compute panel (a).

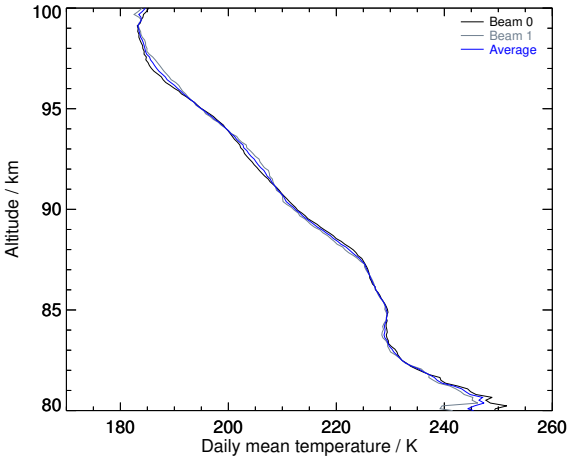

(c) Mean temperature profiles measured by the Na lidar's beam 0, beam 1, and the average of these.

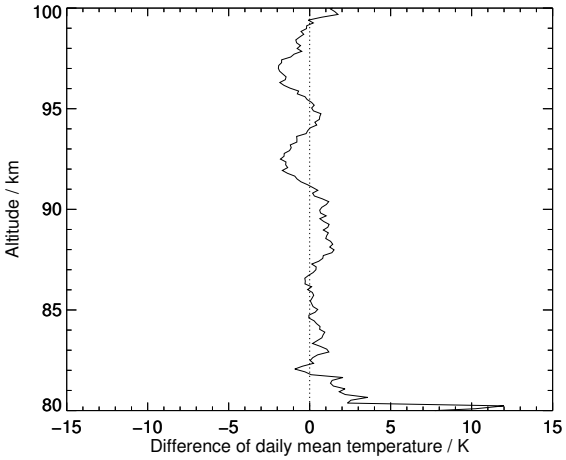

(d) Mean profile of the temperature difference between beam 0 and beam 1, shown in panel (c).

Figure S43: 2014–01–27

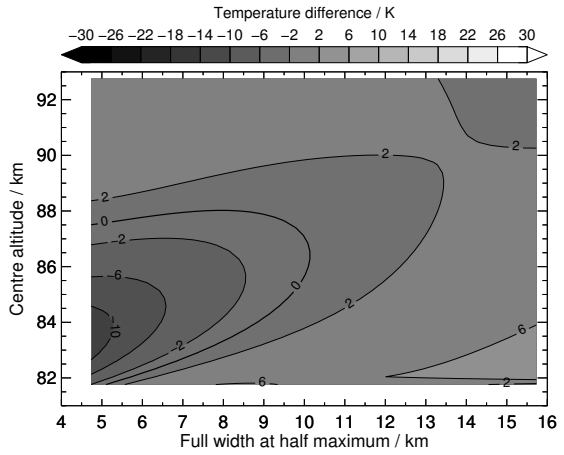

(a) Mean temperature difference between data measured by GRIPS 9 and the Na lidar at ALOMAR.

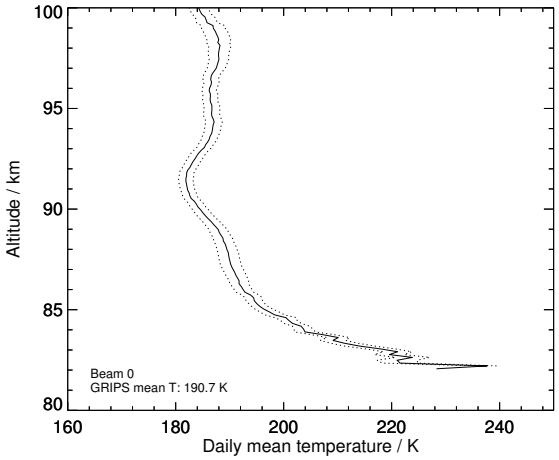

(b) Mean temperature profile from the beam with the best statistics which was used to compute panel (a).

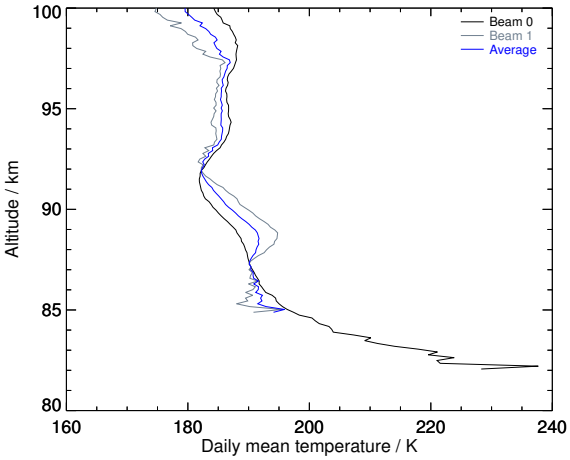

(c) Mean temperature profiles measured by the Na lidar's beam 0, beam 1, and the average of these.

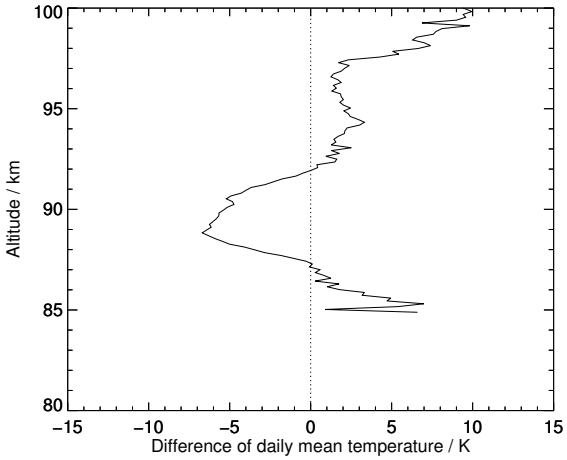

(d) Mean profile of the temperature difference between beam 0 and beam 1, shown in panel (c).

Figure S44: 2014–01–29

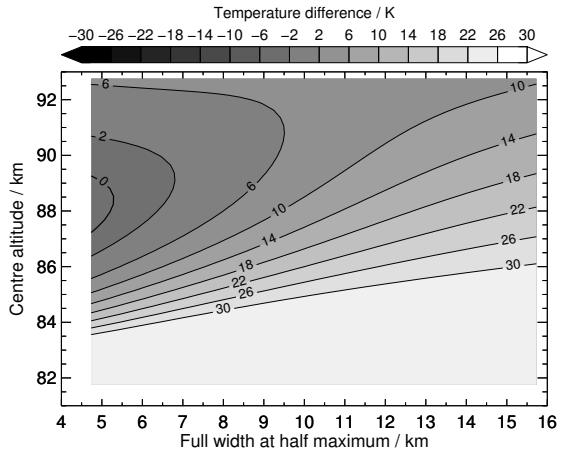

(a) Mean temperature difference between data measured by GRIPS 9 and the Na lidar at ALOMAR.

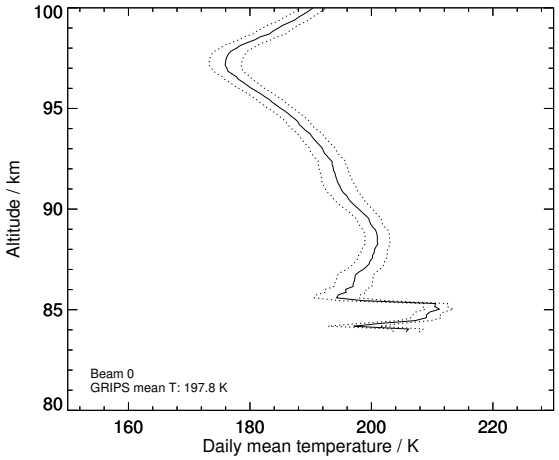

(b) Mean temperature profile from the beam with the best statistics which was used to compute panel (a).

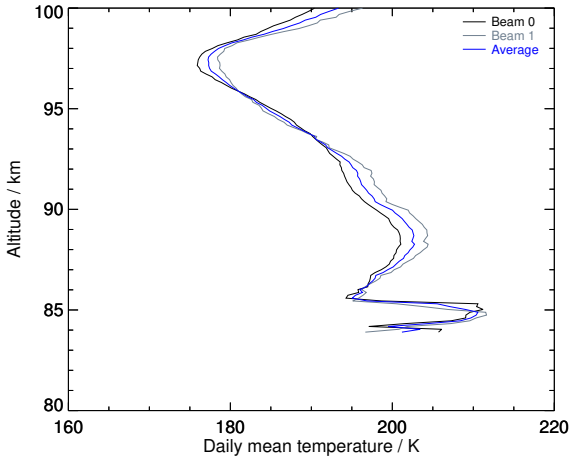

(c) Mean temperature profiles measured by the Na lidar's beam 0, beam 1, and the average of these.

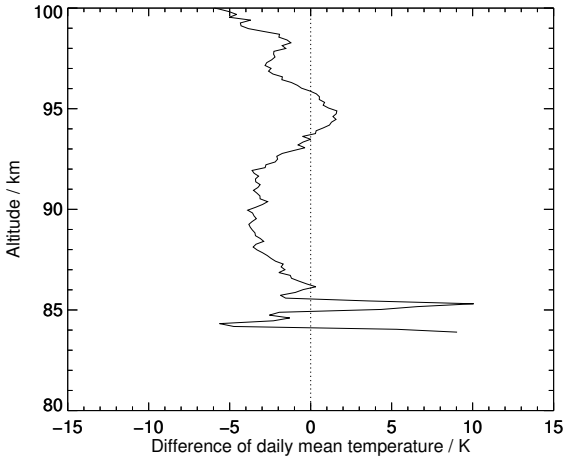

(d) Mean profile of the temperature difference between beam 0 and beam 1, shown in panel (c).

Figure S45: 2014–01–30

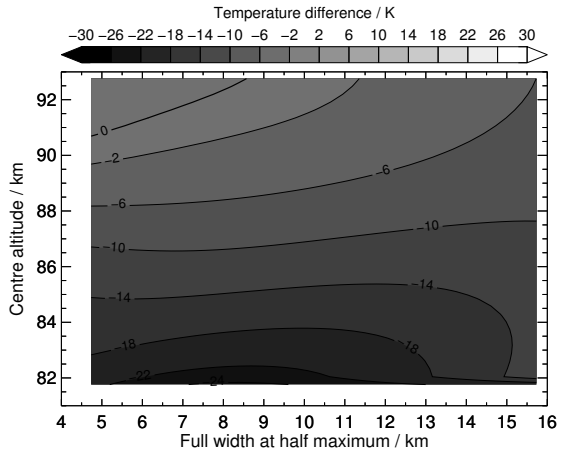

(a) Mean temperature difference between data measured by GRIPS 9 and the Na lidar at ALOMAR.

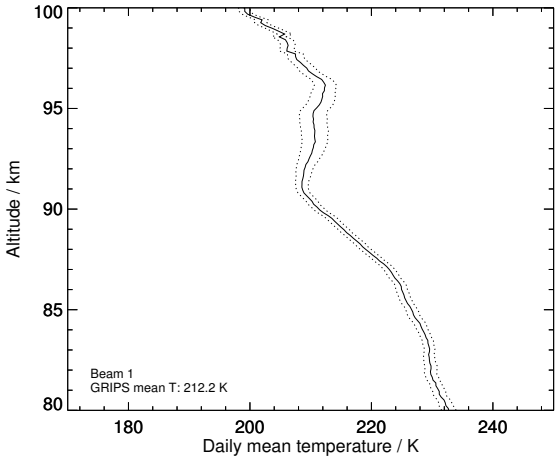

(b) Mean temperature profile from the beam with the best statistics which was used to compute panel (a).

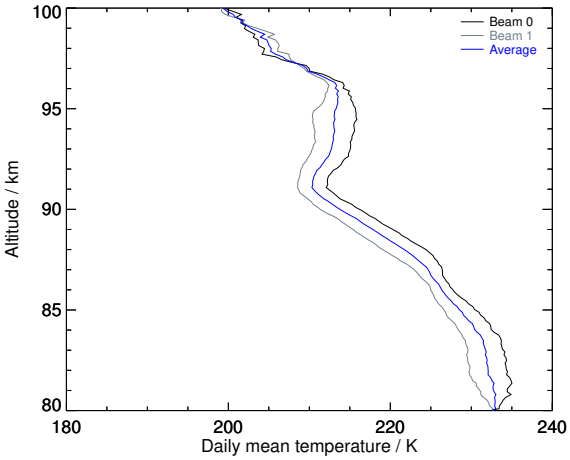

(c) Mean temperature profiles measured by the Na lidar's beam 0, beam 1, and the average of these.

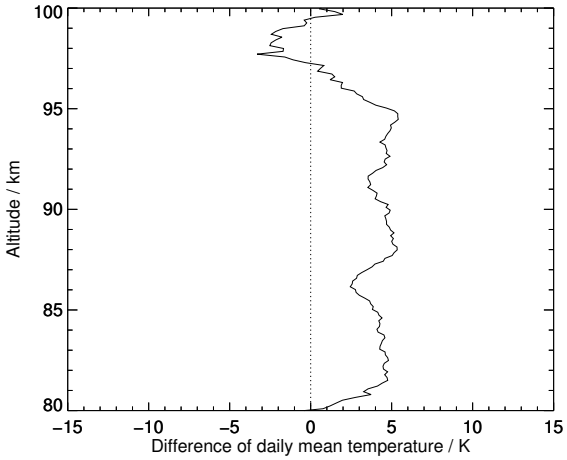

(d) Mean profile of the temperature difference between beam 0 and beam 1, shown in panel (c).

Figure S46: 2014–02–11

References

Baker, D. J., B. K. Thurgood, W. K. Harrison, M. G. Mlynczak, and J. M. Russell (2007). Equatorial enhancement of the nighttime OH mesospheric infrared airglow. *Phys. Scr.* 75(5), pp. 615–619. DOI: 10.1088/0031-8949/75/5/004.

French, W. J. R. and F. J. Mulligan (2010). Stability of temperatures from TIMED/SABER v1.07 (2002–2009) and Aura/MLS v2.2 (2004–2009) compared with OH(6–2) temperatures observed at Davis Station, Antarctica. *Atmos. Chem. Phys.* 10(23), pp. 11439–11446. DOI: 10.5194/acp-10-11439-2010.

Noll, S., W. Kausch, S. Kimeswenger, S. Unterguggenberger, and A. M. Jones (2016). Comparison of VLT/X–shooter OH and O_2 rotational temperatures with consideration of TIMED/SABER emission and temperature profiles. *Atmos. Chem. Phys.* 16(8), pp. 5021–5042. DOI: 10.5194/acp-16-5021-2016.

Pautet, P.-D., M. J. Taylor, W. R. Pendleton, Y. Zhao, T. Yuan, R. Esplin, and D. McLain (2014). Advanced mesospheric temperature mapper for high–latitude airglow studies. *Appl. Opt.* 53(26), pp. 5934–5943. DOI: 10.1364/AO.53.005934.

Swenson, G. R. and C. S. Gardner (1998). Analytical models for the responses of the mesospheric OH^* and Na layers to atmospheric gravity waves. *J. Geophys. Res.–Atmos.* 103(D6), pp. 6271–6294. DOI: 10.1029/97JD02985.

Winick, J. R., P. P. Wintersteiner, R. H. Picard, D. Esplin, M. G. Mlynczak, J. M. Russell III, and L. L. Gordley (2009). OH layer characteristics during unusual boreal winters of 2004 and 2006. *J. Geophys. Res.–Space* 114(A2), A02303. DOI: 10.1029/2008JA013688.

Zhang, S. P., R. G. Roble, and G. G. Shepherd (2001). Tidal influence on the oxygen and hydroxyl nightglows: Wind Imaging Interferometer observations and thermosphere/ionosphere/mesosphere electrodynamics general circulation model. *J. Geophys. Res.–Space* 106(A10), pp. 21381–21393. DOI: 10.1029/2000JA000363.